Journal of Molecular Structure 1270 (2022) 133929

Contents lists available at ScienceDirect

Journal of Molecular Structure

journal homepage: www.elsevier.com/locate/molstr

Ruthenium(III) and (II) complexes containing pyridine moiety: Synthesis, crystal structure and *in vitro* biological evaluation

Jayanthi Eswaran[a,*], Anusuya Mariappan[a,b], Nagaveni Arumugham[a], Theetharappan Murugan[c], Nattamai sp Bhuvanesh[d], Neelakandan Mallanpillai Anathakrishnan[c], Santhanaraj Daniel[e], Rajakumar Kanthapazham[f,*]

[a] Department of Chemistry, Kongunadu Arts and Science College, Coimbatore, Tamilnadu 641049, India
[b] Department of Chemistry, NGM College, Pollachi, Tamilnadu 642001, India
[c] Chemistry Research Centre, National Engineering College, Kovilpatti, Thoothukudi, Tamil Nadu 628503, India
[d] Department of Chemistry, Texas A&M University, College Station, TX 77843, USA
[e] Department of Chemistry, Loyola College, Chennai, Tamilnadu 600034, India
[f] Nanotechnology Research and Education Centre, South Ural State University, Chelyabinsk 454080, Russia

ARTICLE INFO

Article history:
Received 4 July 2022
Accepted 11 August 2022
Available online 16 August 2022

Keywords:
Ru complexes
Hydrazone Schiff base
Ligand cleavage
DNA/BSA binding
Cytotoxicity
One-pot synthesis

ABSTRACT

In the present study, reaction of tridentate chelating hydrazone Schiff base *N'*-(phenyl(pyridine-2-yl)methylidene)benzhydrazide (HL) with $[Ru^{III}Cl_3(PPh_3)_3]$ afforded ruthenium(III) and ruthenium(II) complexeswith the composition of $[Ru^{III}(L)Cl_2(PPh_3)]$ (**1**), $[Ru^{II}(L)Cl(CO)(PPh_3)]$ (**2**) and $[Ru^{II}(Bp)Cl(CO)(PPh_3)]$ (**3**) (where Bp= benzoyl pyridine) in one pot reaction. The molecular structures of synthesized complexes were examined by single crystal X-ray diffraction technique which revealed that the complexes are neutral in charge with distorted octahedral geometry. Further, the stability of the complexes were calculated theoretically and interaction of them with biomolecules resulted in change in binding energies dramatically. Complexes**1**–**3** were evaluated for their interaction with calf thymus DNA (CT DNA) and bovine serum albumin (BSA) using theoretical as well as spectral techniques. In addition, the *in vitro* cytotoxic potential of the synthesised compounds were investigated against human breast cancer cell models (MCF-7 and MDAMB-453).

1. Introduction

Various types of cancer are treated with cisplatin and its derivatives. In spite of their widespread clinical use, these complexes suffer from severe toxic side effects and have acquired drug resistance [1]. Thus, there are continuing efforts to develop new bioactive metal complexes as modern therapeutics. In general, most of the drug industries focused on DNA binding studies. Since, the coordination of metal atoms to nucleic acid bases is found to be improved by hydrogen bonding interactions or weakened due to steric interactions, implying that compounds may be designed to target specific nucleotides. Many researchers focused on the synthesis of intercalating molecules, which distort the helical structure of DNA to inhibit enzymes replications.

In the rapidly emerging field of DNA intercalation studies, ruthenium metal intercalators are vital because of their redox and photophysical properties that enable the utilization of different methods to investigate intercalation processes and binding modes that are linked to the structures of both ruthenium complexes and DNA [2]. Interestingly, the anticancer properties of ruthenium complexes have received much interest in recent years, owing to the fact that several of them have shown promising pharmacological outcomes *in vitro* and *in vivo* in various models, including platinum-resistant cell lines [3]. Clinical trials for Ru(III) complexes bonded with new anti-tumour metastasis inhibitors (NAMI-A) and KP-1339 for development in various drug industries are currently underway [4]. In addition, the axial ligands are crucial to the pharmacological activity of these complexes [5]. NAMI-A binds significantly to human serum albumin (HSA), whereas KP-1019 is more selective in its non-covalent interaction with the hydrophobic regions of HSA, which are crucial in determining the pharmacological properties and effectiveness of these agents. Apparently, the weaker association of KP-1019 causes greater cellular absorption and makes it active against primary cancers [6]. It is more effec-

* Corresponding author.
* During the submission of the manuscript only one author was given permission to be a corresponding author.so In this stage we are adding.
E-mail addresses: jayakumar.jayanthi@gmail.com (J. Eswaran), kantkhapazhamr@susu.ru (R. Kanthapazham).

https://doi.org/10.1016/j.molstruc.2022.133929
0022-2860/

tive in inducing apoptosis against colorectal tumour cell lines than the clinically available drugs 5-fluorouracil and cisplatin [7], while NAMI-A exhibits anti-metastatic activity in secondary tumours [8].

Cisplatin's cytotoxicity is primarily determined by its ability to covalently bind to DNA. Though the biological targets and the mode of action of NAMI-A and KP-1019 have not been totally elucidated, it has been found that both the compounds have the ability to target DNA and proteins, indicating multiple pathways from those obtained for cisplatin [9]. It is believed that the pro-drugs KP-1019 and NAMI-A are converted into more active Ru(II) species by reductant molecules such as glutathione, cysteine, and ascorbic acid in the tumour environment that attacks the target cells [10]. Electrochemical experiments support the "activation by reduction" mechanism of Ru(III) complexes to active Ru(II) complexes in the hypoxic and acidic environments of solid tumours [11]. Meanwhile, ruthenium hydrazone complexes are reported with versatile structures and the ability to interact with biomolecular targets such as DNA and protein, which can aid in interpreting the metabolism, transportation, and structure-activity relationship [12]. Our group synthesised and elucidated the *in vitro* pharmacological activity of various transition metal hydrazone complexes [13]. In continuation of this, we herein report the synthesis, characterisation of Ru(III) and Ru(II) triphenylphosphine complexes containing the hydrazone ligand obtained from 2-benzoyl pyridine and benzhydrazide as an anchoring group as well as their interaction with DNA/BSA in terms of antitumor behaviour.

2. Experimental section

2.1. Materials and methods

All the chemicals used in the synthesis of compounds and buffer solution are of analytical grade. The $RuCl_3.\ 3H_2O$ was purchased from Loba Chemie Pvt. Ltd. Triphenylphosphine, 2-benzoyl pyridine, benzhydrazide, ethidium bromide, and 3-(4, 5-Dimethylthiazol-2-yl)−2,5-diphenyltetrazolium bromide (MTT) were purchased from Sigma-Aldrich and used as received. The starting complex, $[RuCl_3(PPh_3)_3]$, and N'-(phenyl(pyridine-2-yl)methylidene)benzhydrazide (HL) [14], were prepared as previously described [15]. The protein-free calf-thymus DNA (CT-DNA), acquired from Sigma-Aldrich chemicals was stored at 0 - 4 °C. The purity of CT-DNA was determined by measuring its optical density prior to its usage. To prepare the Tris–HCl buffer (5 mM Tris–HCl, 50 mM NaCl, pH 7.2), double-distilled water was used. The DNA stock solutions were prepared freshly before it is used with the buffer solution. Human breast cancer cells (MCF-7 and MDAMB-453) were collected from the National Centre for Cell Science (NCCS), Pune, India. The other chemicals and reagents that were employed for the biological studies were of high grade and were purchased from reputed suppliers.

2.2. Characterization of the complexes

Elemental analyses (C, H, and N) were carried out using the Vario EL III Elemental analyser instrument. The IR spectra (4000–400 cm^{-1}) of the samples were recorded as KBr discs using a Nicolet Avatar FT-IR spectrometer. The melting points of the compounds were measured using the Raaga equipment and the results are uncorrected. Electronic absorption spectra of the materials were obtained using Jasco V-630 spectrophotometer. Emission spectroscopy was employed using the Jasco FP 6600 spectrofluorometer. The ^{1}HNMR spectra were acquired using tetramethylsilane as an internal standard and $CDCl_3$ as a solvent on a high-resolution Bruker Avance 400 spectrometer operating at 400 MHz. The room temperature EPR spectrum of low spin ruthenium(III) complex was recorded using the JES-X3 SERIES EPR spectrometer at an X-band frequency for a powder sample at 278 K with a microwave power of 0.99800 [mW] and the field calibrated with 2,2-diphenyl-1-picrylhydrazyl radical (DPPH, $g = 2.0037$).

Single crystal X-ray diffraction data of complexes **1** and **3** were collected on BRUKER APEX 2 X-ray (three-circle) diffractometer whereas X-ray diffraction data of complex **2** by BRUKER GADDS X-ray (three-circle) diffractometer. Integrated intensity information was obtained for each reflection by the reduction of data frames with APEX2 programme [16]. SADABS was used to correct the data for absorption effects [17]. A solution was readily obtained by SHELXTL (XS) [18]. All non-hydrogen atoms were refined using anisotropic thermal parameters, whereas hydrogen atoms were positioned geometrically and refined as a riding model. X-seed [19] was used to generate the final data presentation and structural plots for complex **1**, whereas Olex2 was used for complexes **2** and **3** [20]. Table 1 summarises the details pertaining to data collection and the structural refinements.

One-pot synthesis of ruthenium(III) and ruthenium(II) complexes $[Ru^{III}(L)Cl_2(PPh_3)]$ (**1**), $[Ru^{II}(L)Cl(CO)(PPh_3)]$ (**2**) and $[Ru^{II}(Bp)Cl(CO)(PPh_3)]$ (**3**). Scheme 1 depicts the reactions involved in the synthesis of new ruthenium complexes. $[RuCl_3(PPh_3)_3]$ solution (0.497 g; 0.5 mmol) in 20 mL of chloroform was refluxed with an equimolar ratio of ligand **HL** (0.151 g; 0.5 mmol) in methanol (20 mL) for 9 h (Scheme 1). During the course of the reaction, a red product precipitated out, was filtered and recrystallized from the MeOH/$CHCl_3$ mixture, yielding complex 1 as a crystalline block, was analysed by single-crystal X-ray diffraction and designated as $[Ru^{III}(L)Cl_2(PPh_3)]$ **(1)**. TLC analysis of the filtrate revealed the presence of two additional products, which were separated by column chromatography using $CHCl_3$ and $CHCl_3$/MeOH mixture to yield complexes of the composition $[Ru^{II}(L)Cl(CO)(PPh_3)]$ **(2)** and $[Ru^{II}(Bp)Cl(CO)(PPh_3)]$ **(3)** and crystallised in 1:1 methanol/acetonitrile and 1:1 methanol/chloroform mixture to yield brown and red crystals of the complexes **2** and **3**, respectively.

$[Ru^{III}(L)Cl_2(PPh_3)]$ (1). Yield: 48%. Colour: Red. Melting point: 248 °C. Elemental analysis: Found (calcd.) (%) for $C_{37}H_{29}Cl_2N_3OPRu$: C, 60.49(60.52); H, 3.98(3.95); N, 5.72(5.74). Selected IR bands (KBr, ν in cm^{-1}): 1593 & 1488 (C=N–N=C); 1323 (C–O); 1081 (N–N); 1434, 1077, 693 (for PPh_3). ESI-MS: calcd. for $C_{37}H_{29}Cl_2N_3OPRu$ is 734.05; found $[M+H]^-$: 735.08.

$[Ru^{II}(L)Cl(CO)(PPh_3)]$ (2). Yield: 27%. Colour: Red. Melting point: 278 °C. Elemental analysis: Found (calcd.) (%) for $C_{38}H_{29}ClN_3O_2PRu$: C, 62.23(62.25); H, 3.95(3.98); N, 5.88(5.90). Selected IR bands (KBr, ν in cm^{-1}): 1584 & 1490 (C=N–N=C); 1319 (C–O); 1084 (N–N); 1947(C≡O); 1435, 1078, 693 (for PPh_3). ^{1}H NMR ($CDCl_3$, δ ppm) 8.15–6.22 (m, 29H, Ar-H). ESI-MS: calcd. for $C_{38}H_{29}ClN_3O_2PRu$ is 727.07; found $[M+H]^-$: 728.09.

$[Ru^{II}(Bp)Cl(CO)(PPh_3)]$ (3).Yield: 9%. Colour: Brown. Melting point: 118 °C. Elemental analysis: Found (calcd.) (%) for $C_{31}H_{24}Cl_2NO_2PRu$: C, 57.68(57.56); H, 3.75(3.81); N, 2.17(2.19). Selected IR bands (KBr, ν in cm^{-1}): 1593 (C=O); 1480 (C=N); 1942(C≡O); 1433, 1077, 695 (for PPh_3). ^{1}H NMR ($CDCl_3$, δ ppm) 8.21–7.31 (m, 24H, Ar-H). ESI-MS: calcd. for $C_{31}H_{24}Cl_2NO_2PRu$ is 645.45; found $[M+H]^-$: 646.24.

2.3. Frontier molecular orbital theory (FMO) analysis

The crystalline structures of the synthesized complexes were optimised by applying DFT calculations using the B3LYP/6–31 G/LANL2DZ methods of the Gaussian09W computation programme [21]. Specifically, the basic set LANL2DZ was used for the metal ion of the complexes and 6–31 G was applied for the atoms present in the complexes. The Highest Occupied Molecular Orbital (HOMO) and Lowest Unoccupied Molecular Orbital (LUMO) values were taken from the Gaussian output results and the energy gap

Table 1
Experimental data for crystallographic study.

	Complex 1	Complex 2	Complex 3
CCDC deposition no.	897,079	897,082	897,080
Empirical formula	$C_{38}H_{33}Cl_2N_3O_2PRu$	$C_{40}H_{32}ClN_4O_2PRu$	$C_{31}H_{24}Cl_2NO_2PRu$
Formula weight	766.61	768.19	645.45
Temperature (K)	110(2)	110(2)	110(2)
Wavelength (Å)	0.71073	1.54178	0.71073
Crystal system	Triclinic	Triclinic	Triclinic
Space group	*P-1*	*P-1*	*P-1*
Unit cell dimensions			
a (Å)	10.613(4)	10.8217(15)	11.358(6)
b (Å)	10.851(4)	10.8296(14)	11.472(7)
c (Å)	15.778(6)	15.976(2)	12.482(7)
α (°)	95.537(4)	86.009(8)	68.222(5)
β (°)	91.394(4)	89.183(8)	74.084(6)
γ (°)	114.054(4)	65.787(7)	65.881(6)
Volume (Å^3)	1647.5(12)	1703.3(4)	1364.0(13)
Z	2	2	2
Density(calculated) (mg/m^3)	1.545	1.498	1.572
Abs. coefficient (mm^{-1})	0.727	5.230	0.860
F(000)	782	784	652
Reflections collected	18,576	19,061	14,459
Independent reflections	7332 [R(int) = 0.0203]	4736 [R(int) = 0.0477]	6098 [R(int) = 0.0215]
Goodness-of-fit on F^2	1.026	1.009	1.047
Final R indices I>2sigma(I)]	R1 = 0.0244, wR2 = 0.0598	R1 = 0.0290, wR2 = 0.0702	R1 = 0.0260, wR2 = 0.0620
R indices (all data)	R1 = 0.0267, wR2 = 0.0610	R1 = 0.0343, wR2 = 0.0714	R1 = 0.0305, wR2 = 0.0645

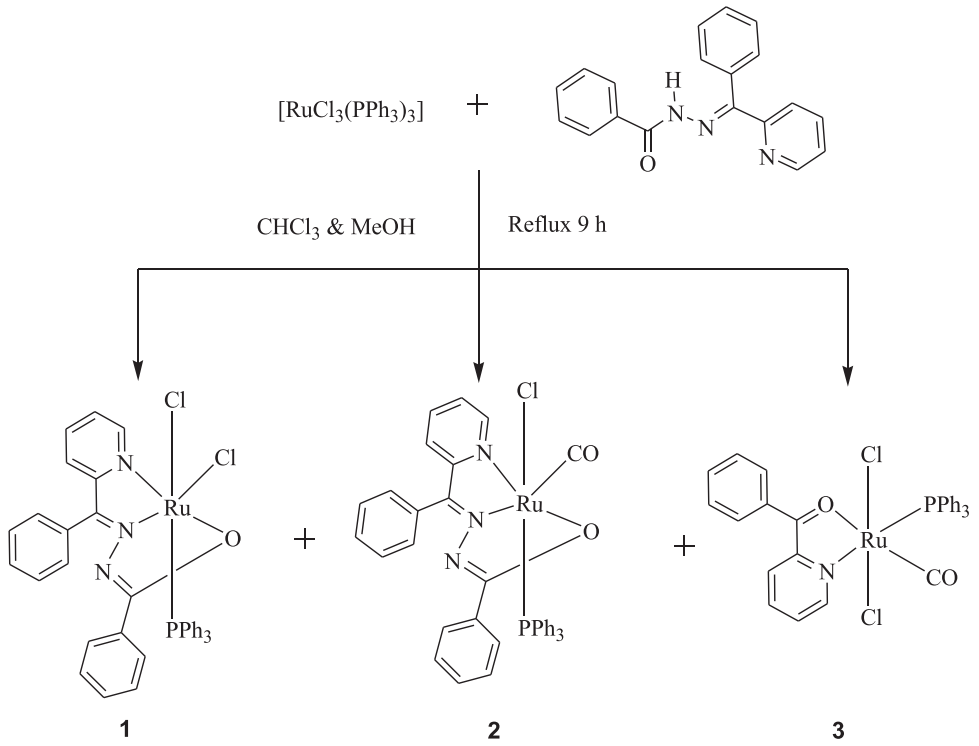

Scheme 1. Synthetic route of ruthenium complexes **1, 2** and **3**.

value was calculated. The frontier molecular orbitals (FMO) have great importance to identify the chemical reactivity and kinetic stability of the complexes [22].

2.4. DNA binding experiments

The concentration of CT-DNA was determined spectrophotometrically using an extinction coefficient of 6600 $M^{-1}cm^{-1}$ at 260 nm. [23]. The solution of CT-DNA in Tris–HCl provided the ratios of UV absorbence of about 1.8–1.9:1 at 260 and 280 nm confirming that the CT- DNA was sufficiently free of protein [24]. The prepared CT-DNA stock solution was stored at 277 K and used upto 4 days only. The corresponding complexes were dissolved in DMSO to prepare the stock solutions, and Tris-buffer was used to dilute the stock solutions to the concentration that is required for the binding experiments.

2.4.1. Absorption titration

In absorption titration studies, the spectra of CT-DNA in the presence and absence of each compound were recorded at a constant complex concentration (25 µM) but with varying nucleotide concentrations ranging from 0 to 25 µM. To monitor the binding

between the complexes, the absorbance (A) band of the complexes that change dramatically owing to the addition of CT-DNA was chosen. The intrinsic binding constant of the complexes (K_b) with CT-DNA was determined from the absorption titration data using the equation [25],

$$[DNA]/(\varepsilon_a - \varepsilon_f) = [DNA]/(\varepsilon_b - \varepsilon_f) + 1/K_b(\varepsilon_b - \varepsilon_f) \quad (1)$$

Through a plot of $[DNA]/[\varepsilon_a - \varepsilon_f]$ versus [DNA], in which DNA is the concentration of DNA in the base pairs. The apparent absorption coefficients ε_a, ε_f and ε_b correspond to A_{obsd}/[Ru], however, the extinction coefficient for the free compounds, and in the fully bound form respectively. The slope and Y intercept of the linear fit of $[DNA]/[\varepsilon_a - \varepsilon_f]$ versus [DNA] give $1/[\varepsilon_b - \varepsilon_f]$ and $1/(K_b[\varepsilon_b - \varepsilon_f])$, respectively. The intrinsic binding constant K_b is the ratio of the slope to the intercept.

2.4.2. Luminescence titration by using ethidium bromide (EB)

Fluorescence spectroscopy was used to examine the competitive interaction of the complexes with EB using an ethidium bromide (EB)-bound CT-DNA solution in Tris–HCl buffer solution (pH, 7.2). The changes in the fluorescence spectral intensities of DNA bound EB at 605 nm (545 nm excitation) with respect to complex concentration were measured. In Tris–HCl buffer solution (pH, 7.2), EB was non-emissive due to fluorescence quenching of free EB by solvent molecules. Because of its intercalative binding to DNA, EB showed enhanced emission intensity in the presence of DNA. The displacement of the bound EB caused by competitive binding of the metal complexes to CT-DNA resulted in a reduction in emission intensity. The classical Stern-Volmer equation was used to obtain the quenching constant (Kq) [25],

$$K_{EB}[EB] = K_{app}[complex] \quad (2)$$

where, [EB] = 10 μM and $K_{EB} = 1 \times 10^7$ M^{-1}.

2.4.3. Protein binding studies

Tryptophan fluorescence quenching experiments with bovine serum albumin(BSA) were performed, with the excitation wavelength at 280 nm and corresponding emission at 345 nm assigned to that of BSA, and the changes in emission spectra were monitored by increasing the concentrations of ruthenium complexes as the quencher. All the experiments have been done with the same excitation and emission slit widths and scan rates. A BSA stock solution in 50 mM phosphate buffer (pH = 7.2) was prepared and stored at 4 °C in the dark. The metal complex stock solutions were prepared by dissolving them in DMSO: phosphate buffer (5: 95) and diluting them with phosphate buffer to the required concentrations. One μM BSA solution was titrated by the successive additions of a 2 μM stock solution of complexes using a micropipette.

Titrations were manually done using a micropipette for the addition of the compounds. For synchronous fluorescence spectra also, the same concentrations of BSA and the compounds were used by scanning simultaneously the excitation and emission monochromators, such as $\Delta\lambda$=15 and $\Delta\lambda$=60 nm. Stern–Volmer and Scatchard graphs were used to study the interaction of quencher with serum albumin [26]. According to the Stern–Volmer quenching equation [25],

$$I_0/I = 1 + k_q\tau_0[Q] = 1 + K_{SV}[Q] \quad (3)$$

where, 'I_0' is the initial tryptophan fluorescence intensity of BSA, 'I' is the tryptophan fluorescence intensity of BSA after the addition of the quencher, k_q is the quenching rate constants of protein, K_{SV} is the dynamic quenching constant, τ_0 is the average lifetime of BSA without the quencher, and [Q] is the concentration of the quencher.When small molecules bind independently to a set of equivalent sites on a macromolecule, the equilibrium between free and bound molecules is represented by the Scatchard equation [27],

$$\log[F_0 - F/F] = \log K_{bin} + n\log[Q] \quad (4)$$

where, K_{bin} and n are the binding constant and the number of binding sites, respectively. Thus, a plot of log [F_0-F/F] versus log [Q] is used to determine the values of both the binding constant (K_{bin}) and number of binding sites 'n'.

2.4.4. Molecular docking studies

The metal complexes **1**–**3** were optimized using Gaussian program by B3LYP method. The crystal data of the biomolecules (BSA protein/DNA) were downloaded from Protein Data Bank (http://www.rcsb.org). Docking results were obtained using AutoDock tools v1.5.6 and AutoDock vina software [28]. Optimized structures of complexes **1–3** were converted into PDB format using discovery studio software. The binding interactions and the binding energy values were calculated using Discovery Studio 2017 R2 64-bit Client software. The grid box values were fixed at 60 × 60 × 60 for the respective biomolecules and the grid spacing value of 0.530. The grid box position was used to centre the binding interactions, which almost took up the entire DNA/BSA molecule. To find the most stable binding configuration with maximum interaction mode and binding energy and affinity of the complexes with 6-bp DNA (PDB ID: 1Z3F) and BSA protein (PDB ID: 3V03). From the possible nine conformer structures of the 1–3, they got the PDBQT format to bind with the biomolecule. The least negative energy value conformer is considered as the best binding mode and, using that conformer, the docking study will be carried out.

2.4.5. Cytotoxicity experiment

The anti-proliferative effects of characterised ruthenium complexes against human breast cancer cell lines (MCF-7 and MDAMB-453) were tested using the MTT (3-(4,5-dimethylthiazol-2-yl)−2, 5-diphenyltetrazolium bromide) assay [29]. The cells were seeded at a density of 1106 cells per well in a 96-well sterile tissue culture plate with 150 L of Dulbecco's Modified Eagle's Medium (DMEM) supplemented with 5% FBS and was allowed to attach for 12 h in a humidified CO_2 incubator. The media were aspirated after 12 h of incubation, and the resultant complexes were serially diluted and added at concentrations ranging from 1 to 25 M. Positive controls include a DMSO vehicle control and an untreated cell control, along with the standard drug (cisplatin). After 24 h, the media was removed from the wells and replaced with 100 L of medium containing 20 L of MTT (5 mg/mL PBS (phosphate-buffered saline)) and incubated for 6 h at 37 °C. The MTT-containing medium was emptied after four hours and replaced with a DMSO solubilization solution for 30 min. The mean absorbance for each drug dosage expressed as a percentage of the control untreated well absorbance was plotted against the various drug concentrations as a percentage of the control untreated well absorbance. The IC_{50} values are the drug concentrations that lowered the mean absorbance at 570 nm to 50 % of the untreated control wells, and a graph is plotted with the percentage of cell inhibition versus concentration. From the slope, the IC_{50} value was calculated.

$$\text{Inhibition}(\%) = [\text{mean OD of untreated cells(control)}/\text{mean OD of treated cells}] \times 100 \quad (5)$$

2.4.6. Lactate dehydrogenase leakage(LDH) assay

The LDH activity of complexes 1-3 in terms of plasma membrane damage on MCF-7 and MDAMB-453 cells was assessed by the linear region of a pyruvate standard graph using regression analysis and expressed as percentage of leakage. Cells were seeded at a density of 1×10^7 cells per well in a 24 well sterile tissue culture plate with 1000 L of Dulbecco's Modified Eagle's Medium

(DMEM) supplemented with 5 % FBS and was allowed to attach for 12 h in a humidified CO_2 incubator. After 12 h of incubation, compounds were treated and LDH leakage was determined using an LDH assay kit (Agappe, Kewaral, India) according to the manufacturer's protocol [30].

3. Results and discussion

3.1. Characterization of complexes

The equimolar reaction of $[Ru^{III}Cl_3(PPh_3)_3]$ with N'-(phenyl (pyridine-2-yl)methylidene)benzohydrazide**(HL)** produced complexes with composition $[Ru^{III}(L)Cl_2(PPh_3)]$ **(1),** $[Ru^{II}(L)Cl(CO)(PPh_3)]$ **(2)**, as well as $[Ru^{II}(Bp)Cl(CO)(PPh_3)]$**(3).** The methanol degradation was responsible for the formation of carbon monoxide, which was coordinated in complexes **2** and **3**. Furthermore, ruthenium-assisted hydrazone cleavage resulted in complex **3** containing a coordinated benzoyl pyridine. The resultant analytical data from all three complexes agree well with the proposed molecular formulae. The complexes are stable in air and light, soluble in most of the organic solvents such as CH_2Cl_2, $CHCl_3$, DMF, and DMSO, and have been thoroughly characterized using a variety of physicochemical techniques.

The IR spectrum of the free ligand was compared with ruthenium complexes to investigate the binding mode(s) of the hydrazone ligand to the metal. The vibrations ν(N–H), (C=O), (C=N), and (N–N) produce distinct absorption bands in the ligand spectrum at 3148, 1683, 1578, and 1076 cm^{-1}, respectively. The IR spectra of the complexes differ markedly from those of the free ligands, as described below. In complexes **1** and **2**, the bands due to the presence of (C=O) and (N–H) stretching vibrations are absent in the IR region, and the appearance of two bands between 1593 and 1490 cm^{-1} and 1323–1319 cm^{-1} due to the (C=N–N=C) and (C–O) stretching vibrations, respectively, reveals that the enolization of amide oxygen followed by deprotonation occurred before coordination with the metal [12]. Furthermore, the decrease in (C=N) stretching frequency pertaining to the azomethine nitrogen and the increase in (N–N) IR frequency in contrast to the free ligand (5–8 cm^{-1}) is primarily attributed to an increase in the double bond character balancing the loss of electron density by donation to the ruthenium metal, clearly demonstrating that the coordination of the hydrazone ligand comprises the presence of azomethine nitrogen atom in complexes **1** and **2** [31]. In addition, a band that is detected at 424 cm^{-1} in the spectra of complexes **1** and **2** was identified as the Ru-N bond of the pyridine moiety in the benzoyl pyridine segment of the hydrazone. Furthermore, the existence of the terminally coordinated carbonyl group was revealed in the IR spectra of complex **2** by a strong band observed around 1947 cm^{-1}. The IR spectrum of complex **3** showed characteristic absorbance bands at 1593, 1480, and 1942 cm^{-1} owing to the stretching vibrations of (C=O), (C=N), and (CO), respectively. The absence of vibration due to -NH and -N-N suggested the absence of hydrazone ligand in the complex **3**.

The ^1H NMR spectra of the complexes **2** and **3** showed significant overlap of signals as a multiplet in the range of 8.15–6.22 and 8.21–7.31 ppm due to the aromatic protons of the ligand as well as triphenylphosphine, respectively. The electronic spectra of all three complexes recorded in DMSO: buffer solution exhibited two or three bands in the range of 260–410 nm. Bands appearing above 300 nm were attributed to $n \rightarrow \pi^*$ ligand transitions and ligand to metal charge transfer (LMCT) transitions of the imine group, while higher energy bands appearing below 300 nm were attributed to $\pi \rightarrow \pi^*$ intra-ligand transitions [12].

The low-spin d^5 configuration is an excellent probe of molecular structure and bonding. The observed "g" values are very sensitive to small changes in the structure and metal-ligand covalency. The solid state EPR spectrum of the powdered sample of complex **1** was recorded at room temperature in order to investigate its paramagnetic nature. On the other hand, complexes **2** and **3** were EPR inactive. The EPR spectrum of complex **1** showed a single isotropic line with a g value of 2.151 ($g_x=g_y=g_z$) (Fig. S1). Although the complex octahedral geometry was distorted, the presence of an anisotropic line in the EPR spectrum might be attributed to the intramolecular spin exchange, which can broaden the lines, or to the occupancy of the unpaired electron in a degenerate orbital [32].

Single-crystal X-ray diffraction technique was employed to examine the exact structures of the complexes. The diffraction data for all three complexes is given in Table 1, and the selected bond lengths and angles are summarised in Table 2. And, the crystalline structure of the complexes is presented in Fig. 1.

3.1.1. Crystallographic study of complex **1**

The crystallisation of complex **1** from a methanol/chloroform mixture produced red blocks with a monometallic structure that included a molecule of methanol in lattice sites that did not interact with the ruthenium centre. Complex **1** crystallized in the triclinic lattice with a P-1 space group and observed two molecules in each unit cell. The crystal structure revealed that the complex **1** was composed of $[Ru^{III}(L)Cl_2(PPh_3)]$ with an octahedral geometry formed by bonding with a tridentate ONN donor hydrazone molecule that formed two five-member chelate rings with bite angles of [N(1)-Ru(1)-O(1) = 76.66(6) °] and [N(1)-Ru(1)-N(3) = 78.68(6) °]. The hydrazone ligand occupied three of the four coordination sites in the basal plane via the pyridine-N, amide-N, and carbonyl-O groups; however, a chloride ion occupied the fourth site. A phosphorus atom from a triphenylphosphine unit and a chloride ion occupy the apical positions, thus forming the distorted octahedron. The charge of the ruthenium (III) centre is fulfilled by two chloride ions and the deprotanatedimidolate oxygen of the hydrazone ligand. The *cis* bond angles (76.66°−105.96°) and *trans* bond angles (153.51°−173.93°) deviate from ideal octahedral angles of 90° and 180°, thus implying distortion in the octahedral geometry. The variation in bond lengths between ruthenium and various donor atoms, which range from 1.978(2) to 2.4178(7), further demonstrates the distortion. Further,inter-molecular H-bonding of the basal chloride ion with the lattice methanol was responsible for the increase in bond length [Ru(1)-Cl(2)=2.4178(8)Å] than to the [Ru(1)-Cl(1)= 2.3748(8)Å] present in the apical position.

3.1.2. Crystallographic study of complex 2

The unit cell dimensions clearly show that the crystal system is triclinic that belongs to the space group *P-1*. The asymmetric unit consists of two independent molecules with almost similar geometrical parameters. Ruthenium(II) atoms are hexa-coordinated with $N_2ClOP(CO)$ donor atoms and slightly distorted from octahedral geometry.The ligand's pyridine-N, amide-N, and carbonyl-O occupy three sites in the basal plane, forming a set of five member chelate rings with bite angles [N(1)-Ru(1)-O(1) = 76.46 (9%)] and [N(1)-Ru(1)-N(3) = 79.26 (9%)].whereas the fourth site is engaged by a terminally coordinated carbonyl ligand. A phosphorus atom from a triphenylphosphine unit and a chloride ion inhabit the apical positions to complete the distorted octahedron. The carbonyl group occupies the site trans to the ligand's N1 imine nitrogen [(C(20)-Ru(1)-N(1) = 173.91(11)].

It could be due to the strong Ru(II)→CO back donation, as shown by the short Ru–C bond (1.873(2)) that prefers the weak donor groups occupying the site opposite to CO, which could also favour the d– π^* back donation.The length of the Ru–C bond in Ru (CO) complexes was found to be 1.873 A, which was very similar to that of ruthenium complexes [33]. The Ru(II) centre is satisfied by a chloride ion and a deprotonated imidolate oxygen atom. The

Table 2
Selected bond lengths (Å) and bond angles (°).

Complex 1		Complex 2		Complex 3	
Bond Length					
Ru(1)-N(1)	1.9775(15)	Ru(1)-C(20)	1.873(3)	Ru(1)-C(13)	1.874(2)
Ru(1)-O(1)	2.0277(13)	Ru(1)-N(1)	2.022(2)	Ru(1)-N(1)	2.1162(18)
Ru(1)-N(3)	2.0490(15)	Ru(1)-N(3)	2.062(2)	Ru(1)-O(1)	2.1776(15)
Ru(1)-P(1)	2.3337(8)	Ru(1)-O(1)	2.0884(19)	Ru(1)-P(1)	2.3109(11)
Ru(1)-Cl(1)	2.3748(8)	Ru(1)-P(1)	2.2919(9)	Ru(1)-Cl(1)	2.3840(12)
Ru(1)-Cl(2)	2.4178(8)	Ru(1)-Cl(1)	2.4553(8)	Ru(1)-Cl(2)	2.3848(14)
Bond angle					
N(1)-Ru(1)-O(1)	76.66(6)	C(20)-Ru(1)-N(1)	173.91(11)	C(13)-Ru(1)-N(1)	97.93(8)
N(1)-Ru(1)-N(3)	78.68(6)	C(20)-Ru(1)-N(3)	99.95(11)	C(13)-Ru(1)-O(1)	173.05(7)
O(1)-Ru(1)-N(3)	153.51(5)	N(1)-Ru(1)-N(3)	79.26(9)	N(1)-Ru(1)-O(1)	75.61(7)
N(1)-Ru(1)-P(1)	98.00(5)	C(20)-Ru(1)-O(1)	104.18(11)	C(13)-Ru(1)-P(1)	87.44(7)
O(1)-Ru(1)-P(1)	81.90(4)	N(1)-Ru(1)-O(1)	76.46(9)	N(1)-Ru(1)-P(1)	174.51(4)
N(3)-Ru(1)-P(1)	92.12(4)	N(3)-Ru(1)-O(1)	155.71(9)	O(1)-Ru(1)-P(1)	99.07(6)
N(1)-Ru(1)-Cl(1)	171.62(4)	C(20)-Ru(1)-P(1)	90.97(9)	C(13)-Ru(1)-Cl(1)	95.73(7)
O(1)-Ru(1)-Cl(1)	105.95(4)	N(1)-Ru(1)-P(1)	95.12(7)	N(1)-Ru(1)-Cl(1)	88.39(5)
N(3)-Ru(1)-Cl(1)	99.83(4)	N(3)-Ru(1)-P(1)	96.91(7)	O(1)-Ru(1)-Cl(1)	81.67(5)
P(1)-Ru(1)-Cl(1)	90.28(4)	O(1)-Ru(1)-P(1)	85.47(6)	P(1)-Ru(1)-Cl(1)	92.20(3)
N(1)-Ru(1)-Cl(2)	83.15(5)	C(20)-Ru(1)-Cl(1)	90.08(9)	C(13)-Ru(1)-Cl(2)	94.39(6)
O(1)-Ru(1)-Cl(2)	92.61(4)	N(1)-Ru(1)-Cl(1)	83.87(7)	N(1)-Ru(1)-Cl(2)	85.04(5)
N(3)-Ru(1)-Cl(2)	93.94(4)	N(3)-Ru(1)-Cl(1)	89.11(7)	O(1)-Ru(1)-Cl(2)	87.67(5)
P(1)-Ru(1)-Cl(2)	173.933(15)	O(1)-Ru(1)-Cl(1)	88.17(6)	P(1)-Ru(1)-Cl(2)	93.46(2)
Cl(1)-Ru(1)-Cl(2)	88.74(4)	P(1)-Ru(1)-Cl(1)	173.62(3)	Cl(1)-Ru(1)-Cl(2)	168.604(19)

results were confirmed that a molecule of acetonitrile is solvated in the complexes. More importantly,the *cis* (76.46 (9)−104.18 (11) °) and *trans* bond angles (155.71 (9)−173.91 (11) °) between ruthenium and equatorial and axial ligands in the complex are not close to the ideal angles of a perfect octahedron, confirming the distortion in octahedral geometry [34].

3.1.3. Crystallographic study of complex 3

As the reaction mixture was slowly evaporated at room temperature, Complex **3** was obtained as brown crystals. Each asymmetric unit has two independent molecules that are crystallised in the triclinic space group *P-1*. The molecular structure from the crystallographic studies showed that the coordination sphere around Ru(II) is $NOCl_2P$ (CO). The ORTEP diagram of the complex revealed that the Ru(II) ion possesses a distorted octahedral geometry, with the equatorial plane occupied by a carbonyl oxygen atom and pyridine nitrogen from the benzoyl pyridine moiety, a terminally coordinated carbonyl ligand, and a phosphorous atom from the triphenylphosphine group. The axial positions are occupied by two *trans* chloride ions. As we expected, the two *trans* Ru-Cl bond lengths are much longer than the four equatorial bond lengths due to considerable axial distortion in the complexes.Two central bond lengths [Ru1-Cl1 = 2.3840 (12)] and [Ru1-Cl2 = 2.3848 (14)] are longer than those of the other four basal planar bonds [Ru(1)-C (13) = 1.874(2)], [Ru(1)-N (1) = 2.1162 (18)], [Ru(1)-O (1) = 2.1776 (15)], and [Ru(1)-P (1) = 2.3109 (11)]. The trans angle [Cl(1)-Ru(1)-Cl(2)] deviates from the ideal value of 180°, indicating axial distortion. Further, the other trans angles of the basal planes are limited by the meridional ligands, indicating that the ruthenium metal centre is in deformed octahedral geometry. An interesting observation here was that ruthenium mediated cleavage of C=N of the ligand **HL** during the course of the reaction to afford 2-benzoyl pyridine that was subsequently coordinated to ruthenium as a neutral bidentate ligand. This is due to the possible enolimine and ketoamine tautomerism of the Schiff bases [35]. In contrast, not even a trace of 2-benzoyl pyridine was obtained by heating the ligand **HL** in the same solvent (methanol) for over 10 h. Hence, it was clear that the cleavage of the hydrazone ligand **HL** was facilitated only in the presence of ruthenium metal. Similar behaviour was reported in the case of reactions between metal salts/precursors and Schiff bases [36].

3.1.4. Proposed mechanism for the formation of complexes 2 and 3

Complex **1** is the expected product of the reaction when the coordination mode of the hydrazone ligand is taken into account. The complexes **2** and **3** were formed in the same reaction with a Ru-CO bond in which the ruthenium ion was reduced to a bivalent oxidation state prompted us to investigate their formation. Because formaldehyde can serve as a basic foundation for the carbonyl ligand [37], which can be produced by alcohol oxidation, it was assumed that formaldehyde formed in situ by methanol dehydrogenation (solvent) and served as a source of carbonyl ligand [38]. Further, a carbonyl ligand could stabilise the metal in low-positive or zero-valent oxidation states in metal carbonyl complexes. According to our previous findings, the first-generation Grubbs metathesis catalyst with primary alcohols produced ruthenium monohydride monocarbonyl species [39]. Recently, C.S. Yi et al. reported that the heating of Ru(II) and Ru(III) compounds in the presence of primary alcohols results in the formation of Ru-CO complexes [40]. Ruthenium mediated hydrolytic cleavage of the C=N bond has been previously reported by Mahalingam et al. The hydrazone ligand undergoes cleavage in the C=N bond and is coordinated to the metal ion as a neurtal bidentate ligand through pyridine nitrogen and carbonyl oxygen [37]. Based on these reports, we proposed a possible mechanism to account for their formation in Schemes 2 and 3.

The FMO analysis was performed to determine the structural features of the complexes. The charge density is not uniformly distributed in the HOMO of the complex surface, while it is almost uniformly spared in the LUMO energy level and it is rich in metal atoms. These studies were used to learn about the metal complex's formation. The energy band gap of the metal complexes arenoted in Fig. 2. It reveals that complex **3** can easily form compared with complexes **1** & **2**. The order of the energy gap is **1** > **2** > **3**.

3.2. DNA binding studies (Electronic absorption measurements)

Electronic absorption spectroscopy [41] determines the binding ability of metal complexes with the DNA helix. Transition metal complexes bind to DNA through covalent interactions (in which a labile ligand is replaced with a nitrogen atom of a DNA base, such as guanine N7) or non-covalent interactions (intercalative, electrostatic, and groove binding) [42]. Compounds that bind to DNA by

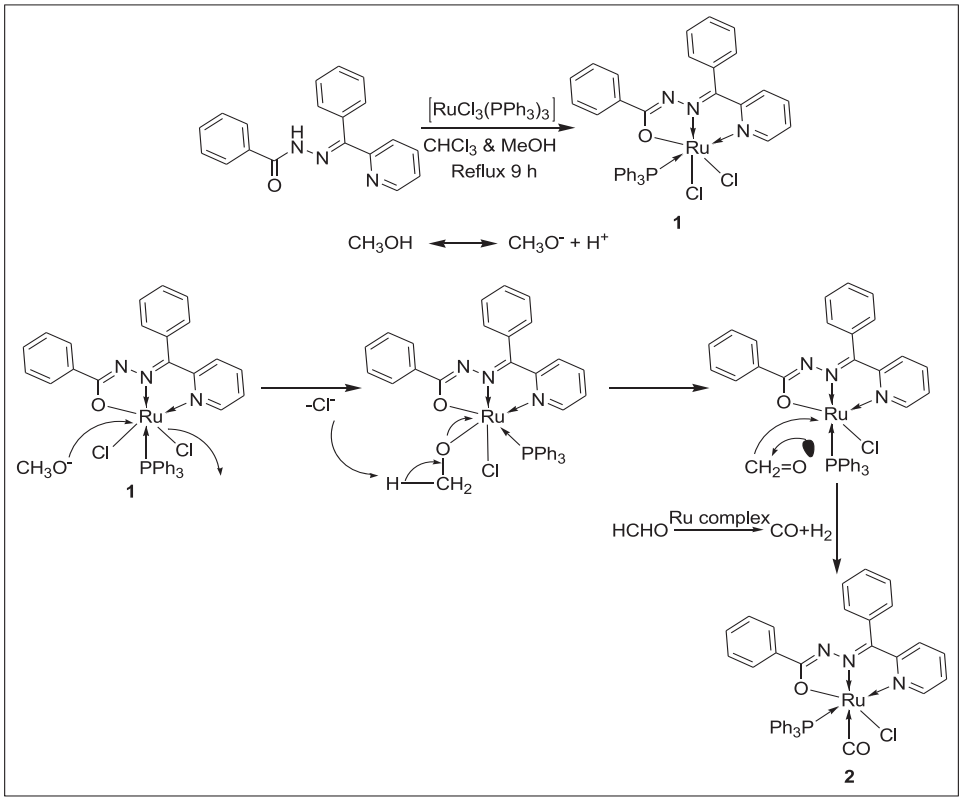

Scheme 2. Proposed mechanism for the formation of complex **2**.

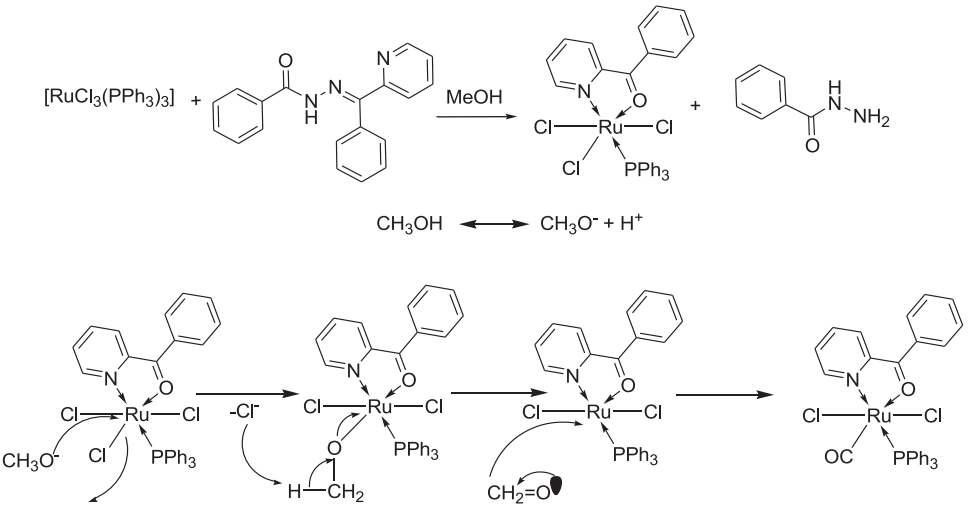

Scheme 3. Proposed mechanism for the formation of complex **3**.

intercalation, which involves a strong stacking interaction between an aromatic chromophore and the base pairs of DNA, alter the latter's double helix structure. They are distinguished by hypochromic and bathochromic shifts. The intensity of hypochromism is usually proportional to the strength of intercalative interaction [41]. Furthermore, the presence of a redshift (bathochromism) indicates that the DNA duplex has stabilised [43]. Electronic spectra of the complexes **1, 2**, and **3** were measured in the presence and absence of CT-DNA and the results are provided in Fig. 3A. The LMCT transitions recorded at 349, 332, and 329 nm were used to investigate the changes in the nature of the absorption bands of corresponding complexes upon the incremental addition of DNA. In the decreasing order corresponding to complexes **1**, **2**, and **3**, the absorption bands exhibited varying degrees of hypochromism of 82, 63, and 36 %, respectively.

Table 3
Absorption and emission spectral data of synthesised complexes.

Complex	$K_b(M^{-1})$	$K_q(M^{-1})$	$K_{app}(M^{-1})$
1	$2.30\pm0.31 \times 10^5$	$3.09\pm0.21 \times 10^4$	$3.04\pm0.43 \times 10^6$
2	$1.03\pm0.19 \times 10^5$	$1.51\pm0.30 \times 10^4$	$1.41\pm0.18 \times 10^6$
3	$7.25\pm0.32 \times 10^4$	$1.29\pm0.19 \times 10^4$	$1.32\pm0.14 \times 10^6$

The intrinsic binding constant (K_b) is a valuable tool for determining and comparing the magnitude of a compound's binding strength to CT-DNA. Table 3 shows the K_b values calculated

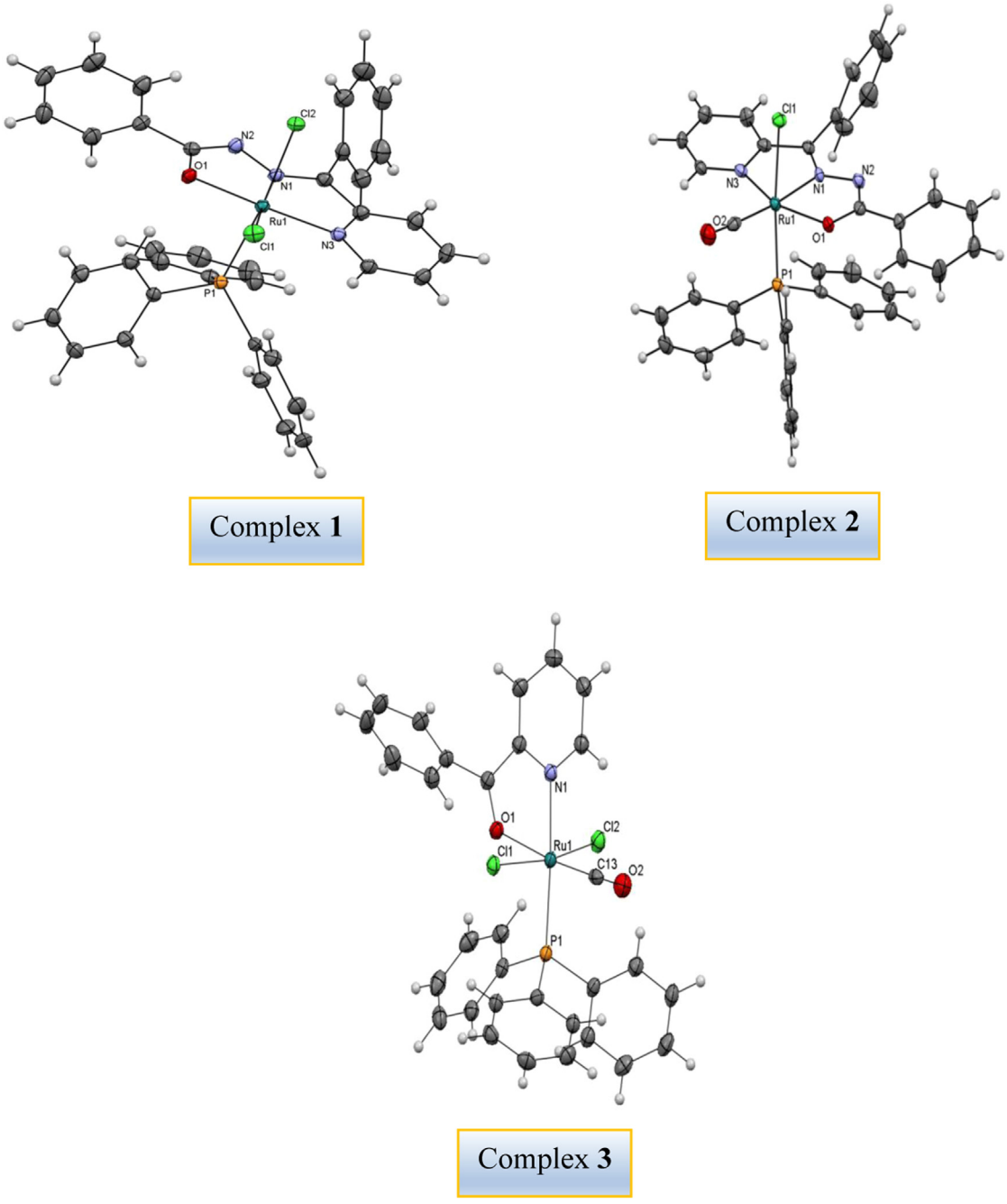

Fig. 1. ORTEP views of ruthenium complexes 1-3 with the atom numbering scheme.

from the plot [DNA]/[a-f] versus [DNA] (Fig. S2).The overall binding affinity of the complexes increased in the order of **3**, **2**, and **1**, respectively**.** According to the observed spectral features and K_b values, all the complexes bind to DNA through the intercalative mode, as previously reported in the study of various metallo-intercalators [27].

3.2.1. Competitive binding between EB and the complexes for CT-DNA

Ethidium bromide (EB) is a typical intercalator, which is a more sensitive fluorescent probe molecule that binds to the DNA through the intercalation process [44]. The competitive binding between the drugs and EB/DNA could provide valuable information about DNA binding affinity. Owing to the strong intercalation of the planar phenanthridinium ring between neighbouring DNA base pairs, EB emits intense fluorescence at around 600 nm. [45]. The experiment focuses on reduction in fluorescence intensity induced by the displacement of EB from a DNA sequence by a quencher, and the quenching is caused by a decrease in the number of binding sites on the DNA which are available for EB. Although the complexes used in this investigation are non-fluorescent at room temperature in solution or in the presence of CT-DNA, their binding to DNA cannot be evaluated directly using emission spectra. EB replacement experiments were carried out to provide evidence for the binding of each complex with DNA. The fluorescence emission spectra of EB bound to DNA in the absence and presence of complexes are shown in Fig. 3B. From the figure, it is clearly evident that there is a significant decrease in the fluorescence intensity of about 47.6, 32.6, and 31.4% together with bathochromic shift on the

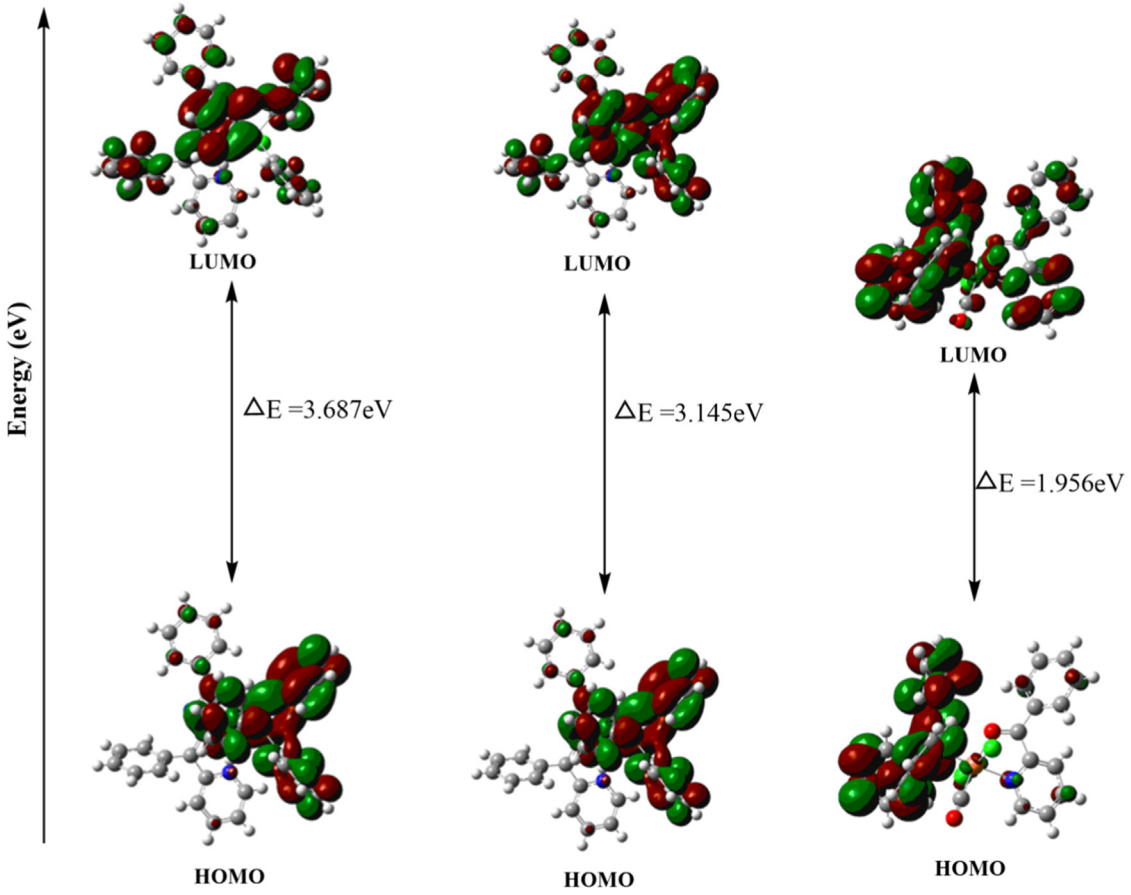

Fig. 2. Frontier molecular orbital diagram of complex **1**–**3**.

addition of complexes **1**, **2**, and **3**, respectively. These results are consistent with the absorption spectral data.

Further, the quenching data were analysed according to the Stern- Volmer equation,

$$I_0/I = K_q[Q]+1 \quad (7)$$

where, $I_0$and I is the absence and presence of emission intensity of quencher. The presence of quencher, K_q is the quenching constant and [Q] is quencher concentration. The K_q value can be obtained from the slope of the plot between I_0/I versus [Q]. The quenching plots show that the quenching of EB bound to CT-DNA by free ligands and complexes agrees well with the linear Stern-Volmer equation. The quenching constant (Kq) is obtained by the slope-to-intercept ratio in the Stern-Volmer plots (Fig. S3.) of I_0/I versus [Q]. The quenching constant(K_q) values and the apparent binding constant values (K_{app}) for complexes **1**, **2** and **3** are given in Table 3. These findings show that the complexes are capable of successfully replacing EB in the EB-DNA complex. The values of the binding and quenching constants increase in the order of **3**, **2**, and **1**. The quenching/binding affinities of bivalent ruthenium complexes **2** and **3** are nearly equal but less than those of trivalent complex **1**. The computed K_q and K_{app} values are higher than those for a few other partial intercalators that have been reported [46]. Nevertheless, it is worth emphasising that the binding ability of the complexes decreases in orders **1**, **2**, and **3**. Though the complexes **1** and **2** are almost identical in their structure, the slight decrease in the binding and quenching constant values of complex **2** compared to complex **1** is responsible for the bivalent oxidation state of the former rather than the trivalent oxidation state of the latter. The trivalent ruthenium complex is a better intercalator than its bivalent counterpart [47].

3.2.2. Protein binding studies

Because of their ability to transport amino acids and drug molecules, serum albumins are the most extensively studied and used in proteins. Hence, the drug–albumin complex is used as a model to understand the basic information regarding their interaction. As a consequence, drug-protein binding studies will assist in the interpretation of a drug's metabolism and transport processes, as well as in understanding the relationship between the structures and functions of a protein.

3.2.3. Fluorescence quenching experiment

Fluorescence quenching measurements have been extensively used to investigate the interactions of metal complexes or small compounds with proteins [48]. In general, fluorescence quenching is the reduction in fluorescence intensity caused by different types of molecular interactions of the drug with the protein, such as ground state complex formation, excited state reactions, and collision quenching. Serum albumin is a protein that improves the apparent solubility of drugs in plasma while simultaneously modulating their transport to cells. As a result, understanding the mechanism of a bioactive compound's interaction with a protein is critical. The nature and magnitude of drug-protein interactions has an influence on the biological activity of drugs, including its effectiveness and rate of delivery [49]. Variations in the molecular environment in the vicinity of the fluorophore may be accessed by changes in fluorescence spectra in the absence and presence of

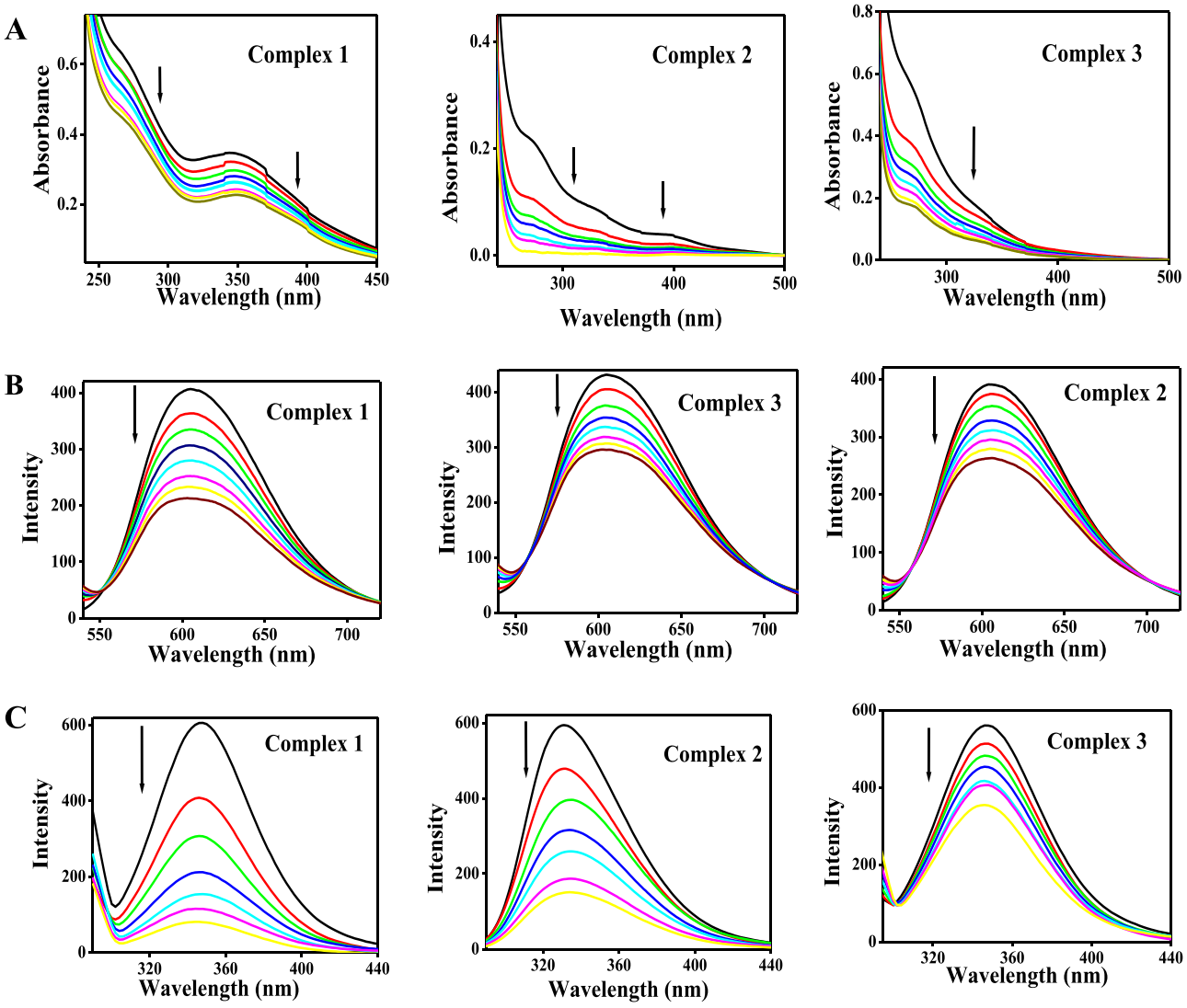

Fig. 3. A 3B and 3C UV–Vis spectra of complexes **1, 2** and **3** in Tris–HCl buffer solution upon the addition of CT-DNA. [Complex]= 25 μM, [DNA] = 0 – 35 Mm and BSA (1 μM; λ_{exi} = 280 nm; λ_{emi} = 346 nm) in the presence of increasing amounts of complexes **1, 2** and **3** (0 – 12 μM). Inserted arrow shows that the emission intensity changes upon increasing complex concentration. Arrow indicates that the absorption intensities decrease upon increasing DNA and complex concentration. UV-Vis spectra of the DNA–EB system, λ_{exi} = 515 nm, λ_{emi} = 530–750 nm, in the presence of complexes **1, 2** and **3**. Concentration of DNA; 10 μM, Complex concentration; 0 – 35 μM, concentration of EB; 10 μM. Inserted arrow shows that the emission intensity changes with respect to the complex concentration.

complexes, providing insights about the nature of the binding phenomenon.

The interaction of BSA with the compounds was investigated using fluorescence measurements at room temperature in the wavelength range of 290-440 nm after excitation at 280 nm. The influence on the fluorescence emission spectrum of BSA (1 M) was titrated with varying concentrations of respective complexes (0–12 M), and the result was illustrated in Fig. 3C. The incremental addition of complexes 1, 2, and 3 to the BSA solution resulted in a reduction of the initial fluorescence intensity of BSA at 345 nm of about 86.7 %, 75.7 %, and 37.7 %, respectively, accompanied by a hypsochromic shift of 2 nm for complexes **1** and **2**. It reveals that the hydrophobicity surrounding tryptophan residues was enhanced, and a bathochromic shift was seen for complex **3**.

The emission spectrum of tryphtophan in the presence of complex **3** undergoes a significant red shift, suggesting that the active site in the protein is located in a more polar environment [50]. Fluorescence quenching mechanisms are typically classified as either static or dynamic. The term "dynamic quenching" refers to a process in which the fluorophore and the quencher come into contact during the excited state's transient existence. On the other hand, static quenching refers to the formation of a fluorophore-quencher complex in the ground state. Electronic spectroscopy is a simple technique for determining the type of quenching. The spectrum for BSA was measured in the absence and presence of the complexes and revealed that there is an increase in BSA absorption intensity with a slight blue shift when the complex was added (Fig. 4). Dynamic quenching, as previously stated, only affected the excited state of the fluorophore and had no effect on the absorption spectrum. The development of a non-fluorescence ground state complex, on the other hand, resulted in a change in the fluorophore's absorption spectrum, indicating that the complex's or ligand's possible quenching mechanism of BSA is a static quenching process [51].

Fig. S4 and Table 4 show the magnitude of the quenching constant (KSV), binding constant (Kb), and the number of binding sites (n) values obtained from the Stern-Volmer and Scatchard plots. According to the values, the hydrazone complexes **1** and **2** interact

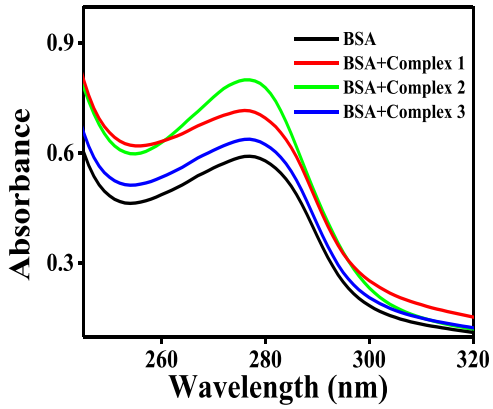

Fig. 4. UV-Vis absorption spectra of BSA (10 μM) with the complexes **1**, **2** and **3**.

Table 4
Emission spectral properties of ruthenium complexes bound to BSA.

Complex	$K_{sv}(M^{-1})$	$K_b(M^{-1})$	n
1	$5.12\pm0.44 \times 10^6$	$2.67\pm0.12 \times 10^6$	1.366
2	$2.68\pm0.28 \times 10^6$	$9.95\pm0.32 \times 10^6$	1.344
3	$4.58\pm0.16 \times 10^4$	$3.75\pm0.29 \times 10^4$	0.990

with BSA more strongly than the one lacking a hydrazone architect (complex **3**). At room temperature, the values of n for all three complexes are close to one, confirming the presence of a single binding site in BSA for the complexes.

3.2.4. Characteristics of synchronous fluorescence spectra

Tryptophan, tyrosine, and phenylalanine are the three fluorophores found in BSA. Tryptophan is the most prominent fluorophore found at substrate binding sites, followed by the tyrosine residue. The investigation of these fluorophore interactions with small molecules can give valuable information about the molecular micro-environment. Additionally, there is evidence that interaction with low molecular weight drugs cause conformational changes in serum albumin, which appear to have an impact on secondary and tertiary protein structures [52]. Synchronous fluorescence spectra reveal details of the molecular microenvironment, particularly in the vicinity of fluorophore functional groups. This method is commonly used to determine the conformational changes in the active binding sites of the protein, that are located near the tryptophan and tyrosine regions. To obtain the information regarding structural changes and the molecular microenvironment, the synchronous fluorescence spectra of BSA were examined before and after the addition of test compounds. Miller's theory states that when the D-value ($\Delta\lambda$) between excitation and emission wavelengths is stabilized at 15 or 60 nm, synchronous fluorescence provides information about tyrosine or tryptophan residues [53].

Fig. 5 depicts the synchronous fluorescence spectra of tyrosine and tryptophan residues in BSA concerning the various concentrations of Ru(II) and Ru(III) complexes added. The addition of complexes **1** and **2** to BSA resulted in an increase in the intensity of tyrosine residue as well as a red shift of 2 and 20 nm, but the addition of complex **3** resulted in a decrease in intensity with a two-nm red shift. In contrast, the addition of ruthenium complexes to BSA resulted in a very small change in the environment around the tyrosine residue. In the case of BSA synchronous fluorescence spectra at $\Delta\lambda$=60 nm, the addition of the corresponding complexes **1**, **2,** and **3** to the solution of BSA resulted in a significant reduction in the fluorescence intensity at 344 nm, up to 88 % , 57 % , and 39 % of the initial fluorescence intensity of BSA, respectively, with no shift in their emission wavelength maxima. According to the above findings, the fluorescence intensity of BSA's tyrosine and tryptophan residues is affected. Therefore, the interaction of complexes with BSA influences the conformation of both the tyrosine and tryptophan regions. However, the effect is most pronounced on the fluorescence intensity of tryptophan residues. The magnitude of the complexes' binding interaction with BSA implies that

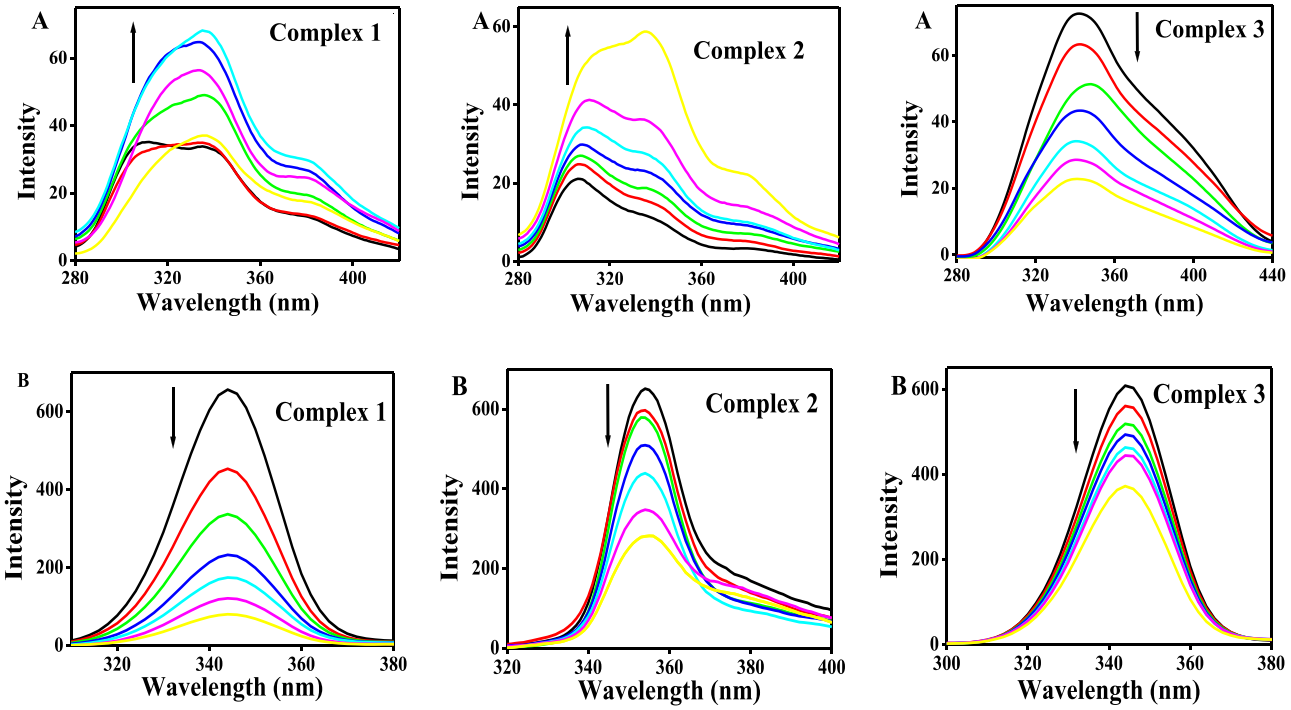

Fig. 5. Synchronous spectra of BSA (1 μM) in the presence of increasing amounts of the complexes **1, 2** and **3** (0-35 μM) at a wavelength difference of $\Delta\lambda$= 15 nm (**A**) and $\Delta\lambda$= 60 nm (**B**). The arrow shows the emission intensity decreases upon the increase in concentration of the complexes.

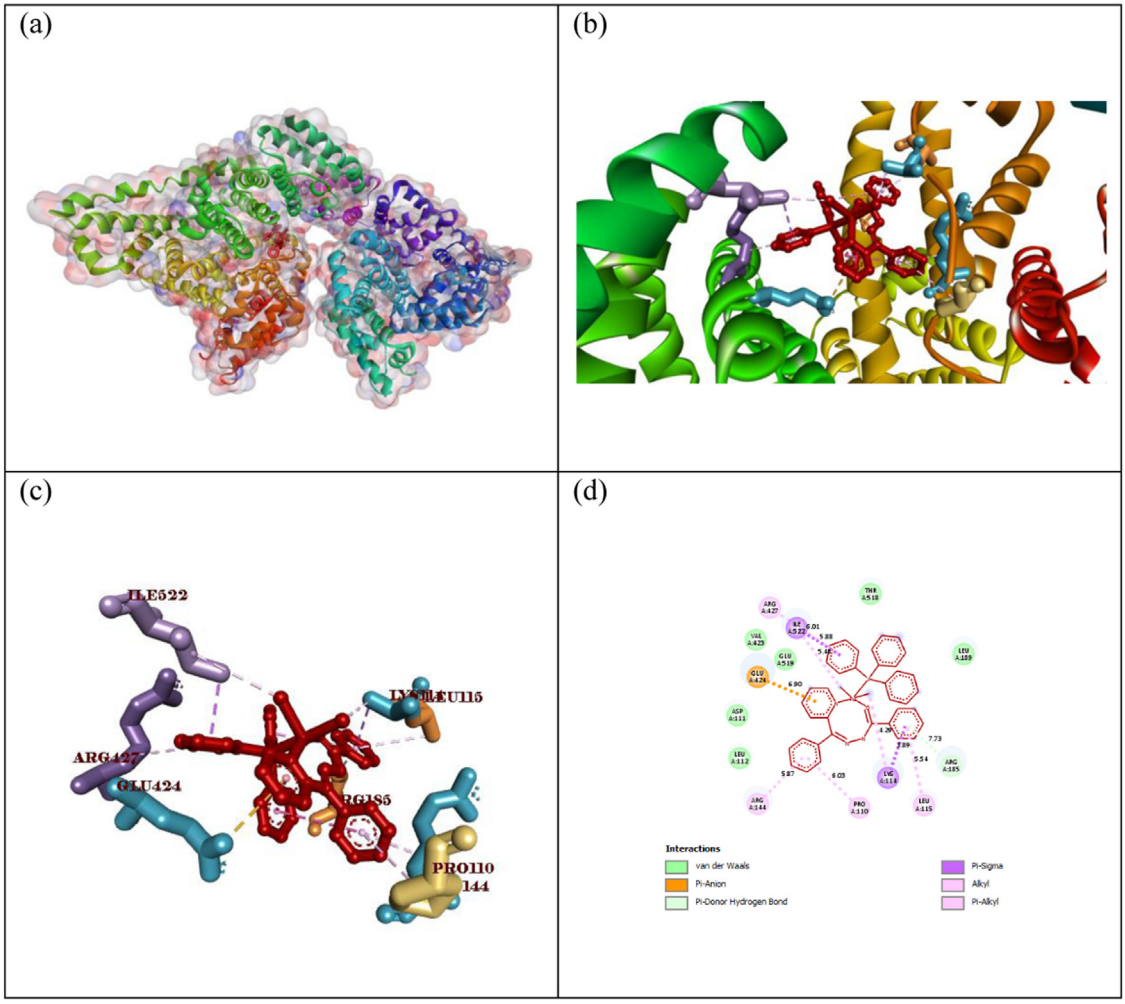

Fig. 6. (a), (b) and (c) represent 3D and specified docking images of complex **2** and d represents 2D specified docking images of complex **2** with BSA.

they can be readily retained in protein and released at specific target sites.

The estimated values of the DNA/BSA binding constant and quenching constants of complexes **1**, **2,** and **3** indicate that biomolecular interactions of complexes are in the increasing order of **3, 2**, and **1** under identical conditions. The complexes **1** and **2** outperformed complex **3** due to the existence of a hydrazone ligand in their architect. Significant binding of these complexes with DNA/BSA as observed in the above experiments prompted us to study the pharmacological properties of these complexes.

3.2.5. Molecular Docking study with BSA protein

The metal complexes **1**–**3** have preferable binding sites to interact with the BSA protein molecule. The binding energy values of the complexes **1**–**3** are, respectively −8.6, −8.1, and −8.4 KJ mol^{-1}. Complex **2** has a greater binding nature towards BSA molecules. The interactions between BSA and the complex **2** with 3D, 2D, and specific binding aspects are shown in Fig. 6, Table 5. Complex **2** interacts with BSA using ILE522, GLU424 and LYS114 majorly. The binding interactions of **1** and **3** are shown in Figs. S5 and S6.

3.2.6. Molecular Docking study with 6-bp DNA with sequence d(CGATCG)2

The molecular docking studies can be added to the typical drug medication outline and theoretical evaluation by putting a little particle into the binding sites of the DNA target specific locale, primarily in a non-covalent mode. The most favoured binding mode of the complexes and possible interactions of the drug with biomolecules were determined using autodock vina. The binding energy values of the metal complexes with DNA were respectively −7.0, −6.7, and −5.5 KJ mol^{-1} for **1**–**3**. In Table 6, the conceivable binding mode, bond distance, and binding sites were shown. From the binding energy values, we can conclude that complex **1** has a higher binding nature towards DNA molecules. Fig. 7 shows the binding interactions of complex **3** with the most suitable binding places in the DNA. The nucleotides DG2 and DG6 are involved in

Table 5
The binding interaction values of complex **1**–**3** with BSA.

ligand	Receptor	Distance A	Binding site
1	**BSA**	4.65	LEU189 – Cl1
		3.90	LVS114 – (C24-C29)
		4.00	LVS114 – (C32-C37)
		3.51	ASP111 – (C7-C12)
2	**BSA**	3.72	ILE522 – (C20-C25)
		4.21	GLU424 – (C1-C6)
		3.73	LYS114 – (C14-C19)
		3.97	LYS114 – Cl2
		4.77	PRO110 – (C7-C12)
3	**BSA**	4.64	ALA349 – (C7-C12)
		3.62	LYS350 – Cl2
		2.58	ARG208 – O1
		1.08	LEU480 – O2
		3.44	ALA209 – Cl1

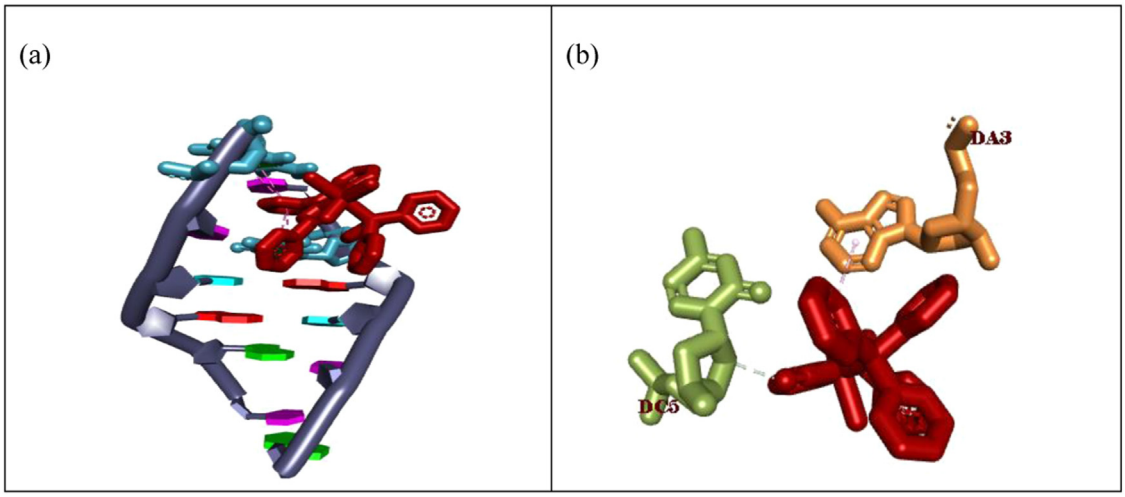

Fig. 7. (a) and (b) represent 3D and 2D specified docking images of complex **3** with DNA.

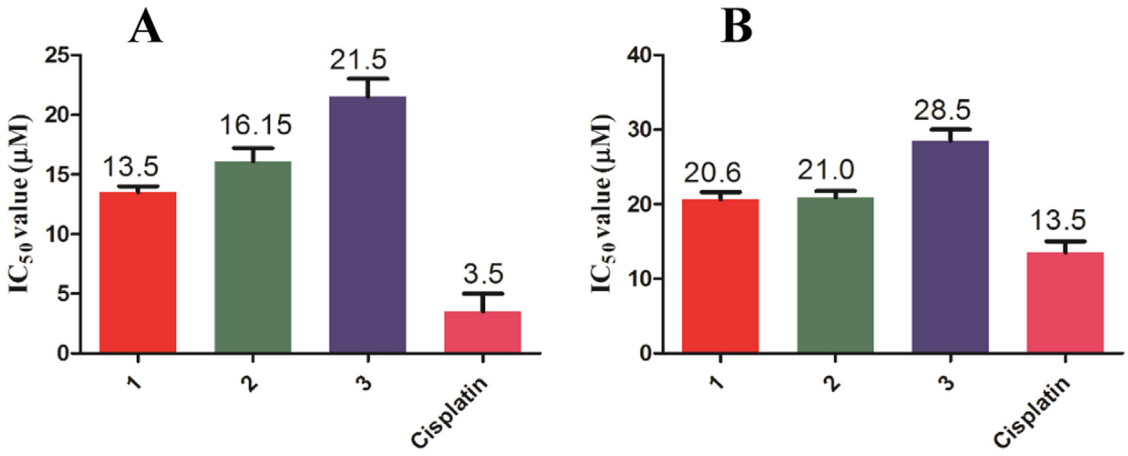

Fig. 8. % Inhibition of human breast cancer MCF-7 (**A**) and MDAMB-453 (**B**) cell lines as a function of concentration of complexes **1**, **2** and **3**.

Table 6
The binding interaction values of complex **1**–**3** with DNA.

Ligand	Receptor	Distance A	Residue
1	**DNA**	5.33	DC5(C7 – C12)
		4.02	DG6(C7 – C12)
		4.54	DG2(C7 – C12)
		5.36	DA3(C7 – C12)
2	**DNA**	4.25	DG2(C7 – C12)
		5.04	DG6(C7 – C12)
3	**DNA**	5.03	DA3 – Cl2
		3.51	DC5 – C1

the binding to **3**. The binding interactions of **1** and **2** are shown in Figs. S7 and S8.

3.2.7. Evaluation of in vitro *anticancer activity (cytotoxicity studies)*

The newly synthesised ruthenium complexes **1**, **2**, and **3** were examined for their cytotoxicity against human breast cancer cell models (MCF-7 and MDAMB-453) by the The MTT assay was used to determine cell viability by measuring the activity of mitochondrial dehydrogenase Fig. 8. *Cisplatin* was used as a positive control. After a 24 h exposure period, the effects of the complexes on the viability of these cells were tested for their anti-tumour activity. All of the complexes showed positive responses, and the corresponding IC_{50} values for 50 % inhibition of tumour cell growth are noted. The cell viability tests revealed that complexes **1**, **2,** and **3** have a greater potential to prevent the growth of MCF-7 cell lines than MDAMB-453 cell lines. Despite the fact that the above mentioned complexes are active against the selected tumour cell lines as evident from *in vitro* cytotoxicity studies, none of them can match the effectiveness of the standard drug *cisplatin*. The results of the cytotoxicity are consistent with the biomolecular interaction results. Complex **3** is relatively less toxic to both the cell lines.

3.2.8. Effect of ruthenium hydrazone complexes on plasma membrane damage (LDH assay)

Apoptosis causes the release of numerous cytoplasmic enzymes. LDH is a stable cytoplasmic enzyme that catalyses the oxidation of lactate to pyruvate and vice versa [54]. It is also a known marker of membrane integrity and a regulator of critical biochemical reactions. The amount of LDH released was analysed in MCF-7 and MDAMB-453 cell lysates in conditioned media for 24 h after treatment with complexes **1**, **2** and **3** (IC_{50} concentrations). Figs. 9 and 10 show the LDH leakage percentage of studied complexes against

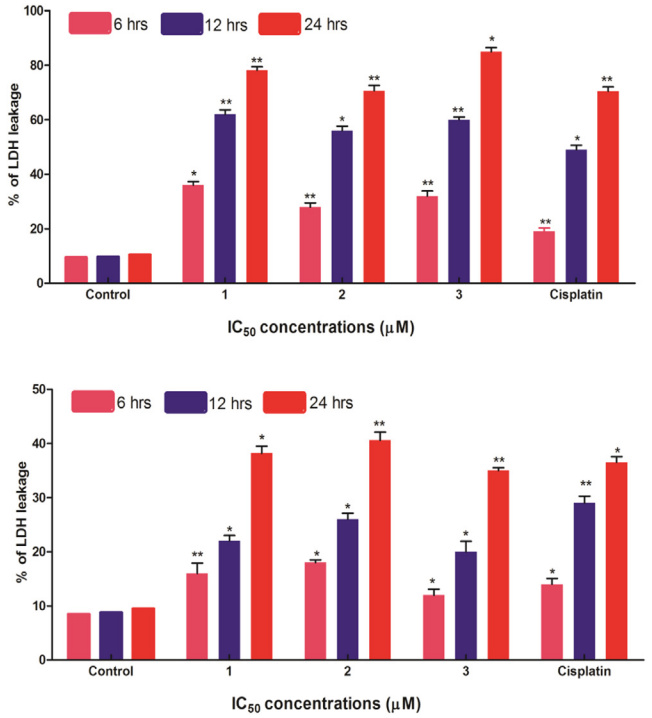

Fig. 9. % of LDH released by MCF-7 cell line after 24 h incubation with IC_{50} concentrations complexes **1**, **2** and **3** (1-complex **1**, 2- complex **2** and 3- complex **3**)with 3 different time intervals (6, 12 and 24 h). The cells were treated with or without IC_{50} concentrations of complexes **1**, **2** and **3** along with the *cisplatin* as a positive drug control for 24 h. Percentage of LDH leakage was measured using LDH assay kit (Agappe, India). Results signify the mean ± SEM of four replicates. $p \leq 0.05$ compared to control.

MCF-7 and MDAMB-453 cells, respectively, at a time interval of 6 h, 12 h, and 24 h. It is thus concluded that the ruthenium complexes caused the death of the studied cancerous cell models by significantly increasing oxidative membrane lipid damage and thus damaging the plasma membrane, resulting in the extracellular release of LDH.

4. Conclusions

The reaction of the hydrazone ligand HL with the starting complex $[Ru^{III}Cl_3(PPh_3)_3]$ in methanol produced the composition's expected complex, $[Ru^{III}(L)Cl_2(PPh_3)]$, as well as a bivalent ruthenium complex, $[Ru^{II}(L)Cl(CO)(PPh_3)]$ **(2)** with a terminally coordinated carbonyl ligand. In addition, the ligand **HL** was cleaved to give 2-benzoyl pyridine that when reacted with the starting complex gave another complex, $[Ru^{II}(Bp)Cl(CO)(PPh_3)]$ (**3**). The spectral and single-crystal XRD studies reveal distorted octahedral geometry for all the synthesised complexes. The results of DNA binding interaction studies provide information that the trivalent ruthenium complex **1** shows better binding propensity. BSA binding interaction studies exhibit static quenching of the complexes. A docking study reveals that all the synthesised metal complexes have a tendency to bind with BSA/DNA. The binding energy values of the complexes 1–3 with BSA are. respectively −8.1, −8.6, and −8.4 KJ mol^{-1} and for DNA, 6.7, 7.0, and 5.5 KJ mol^{-1}.The outcomes of *in vitro* cytotoxicity assays against human breast cancer cell lines (MCF-7 and MDAMB-453) show that complex **1** in the +3 oxidation state is more effective than the other two complexes.

Declaration of Competing Interest

The authors declare that they have no known competing financial interests or personal relationships that could have appeared to influence the work reported in this paper.

Data Availability

The data that has been used is confidential.

Supplementary materials

Supplementary material associated with this article can be found, in the online version, at doi:10.1016/j.molstruc.2022.133929.

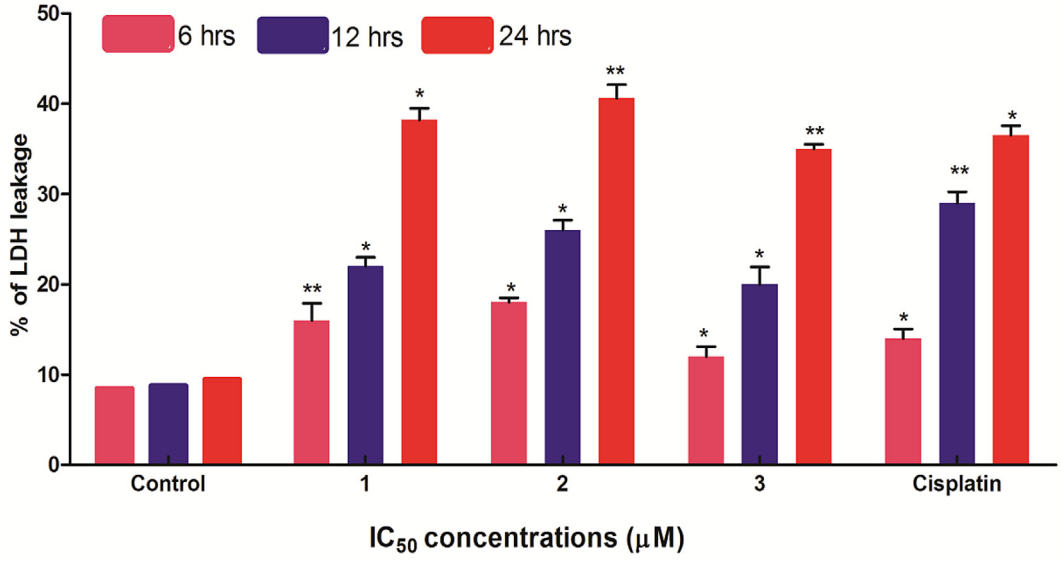

Fig. 10. % of LDH released by MDAMB-453 cell line with IC_{50} concentrations complexes **1**, **2** and **3** (1-complex **1**, 2- complex **2** and 3- complex **3**) with 3 different time intervals (6, 12 and 24 h).Cells were treated with or without IC_{50} concentrations of complexes **1**, **2** and **3** along with the *cisplatin* as a positive drug control for 24 h. Percentage of LDH leakage was measured using LDH assay kit (Agappe, India). Results signify the mean ± SEM of four replicates. $p \leq 0.05$ compared to control.

References

[1] D. Wang, S.J. Lippard, Cellular processing of platinum anticancer drugs, Nat. Rev. Drug Discov. 4 (4) (2005) 307–320, doi:10.1038/nrd1691.

[2] (a) P. Viswanathamurthi, R. Karvembu, V. Tharaneeswaran, K. Natarajan, Ruthenium(II) complexes containing bidentate Schiff bases and triphenylphosphine or triphenylarsine, J. Chem. Sci. 117 (3) (2005) 235–238, doi:10.1007/BF02709292; (b) P. Koepf-Maier, H. Koepf, Non-platinum group metal antitumor agents. history, current status, and perspectives, Chem. Rev. 87 (5) (1987) 1137–1152, doi:10.1021/cr00081a012; (c) C. Metcalfe, J.A. Thomas, Kinetically Inert transition metal complexes that reversibly bind to DNA, Chem. Soc. Rev. 32 (4) (2003) 215–224, doi:10.1039/B201945K; (d) D.L. Carlson, D.H. Huchital, E.J. Mantilla, R.D. Sheardy, W.R. Murphy, A new class of DNA metallobinders showing spectator ligand size selectivity: binding of ligand-bridged bimetallic complexes of ruthenium(II) to calf thymus DNA, J. Am. Chem. Soc. 115 (14) (1993) 6424–6425, doi:10.1021/ja00067a073; (e) Q.X. Zhen, B.H. Ye, Q.L. Zhang, J.G. Liu, L. Hong, L.N. Ji, L. Wang, Synthesis, characterization and the effect of ligand planarity of $[Ru(Bpy)2L]^{2+}$ on DNA binding affinity, J. Inorg. Biochem. 76 (1) (1999) 47–53, doi:10.1016/S0162-0134(99)00107-5.

[3] E.S. Antonarakis, A. Emadi, Ruthenium-based chemotherapeutics: are they ready for prime time? Cancer Chemother. Pharmacol. 66 (1) (2010) 1–9, doi:10.1007/s00280-010-1293-1.

[4] (a) E. Alessio, G. Mestroni, A. Bergamo, G. Sava, Ruthenium antimetastatic agents, Curr. Top. Med. Chem. 4 (15) (2004) 1525–1535, doi:10.2174/1568026043387421; (b) P. Heffeter, K. Böck, B. Atil, M.A. Reza Hoda, W. Körner, C. Bartel, U. Jungwirth, B.K. Keppler, M. Micksche, W. Berger, G. Koellensperger, Intracellular protein binding patterns of the anticancer ruthenium drugs KP1019 and KP1339, JBIC J. Biol. Inorg. Chem. 15 (5) (2010) 737–748, doi:10.1007/s00775-010-0642-1; (c) J.M. Rademaker-Lakhai, D. van den Bongard, D. Pluim, J.H. Beijnen, J.H.M. Schellens, A phase i and pharmacological study with imidazolium-trans-DMSO-imidazole-tetrachlororuthenate, a novel ruthenium anticancer agent, Clin. Cancer Res. 10 (11) (2004) 3717 LP. –3727, doi:10.1158/1078-0432.CCR-03-0746.

[5] G. Mestroni, E. Alessio, G. Sava, S. Pacor, M. Coluccia, A. Boccarelli, Water-soluble ruthenium(III)-dimethyl sulfoxide complexes: chemical behaviour and pharmaceutical properties, Met. Based. Drugs 1 (1) (1994) 41–63, doi:10.1155/MBD.1994.41.

[6] (a) J.B. Aitken, S. Antony, C.M. Weekley, B. Lai, L. Spiccia, H.H. Harris, Distinct cellular fates for KP1019 and NAMI-a determined by X-ray fluorescence imaging of single cells†, Metallomics 4 (10) (2012) 1051–1056, doi:10.1039/c2mt20072d; (b) A. Bergamo, M. Cocchietto, I. Capozzi, G. Mestroni, E. Alessio, G. Sava, Treatment of residual metastases with Na[Trans-RuCl4 (DMSO)Lm] and ruthenium uptake by tumor cells, Anticancer Drugs 7 (6) (1996) 697–702, doi:10.1097/00001813-199608000-00011; (c) C.G. Hartinger, S. Zorbas-Seifried, M.A. Jakupec, B. Kynast, H. Zorbas, B.K. Keppler, From bench to bedside – preclinical and early clinical development of the anticancer agent indazolium trans-[Tetrachlorobis(1H-Indazole)Ruthenate(III)] (KP1019 or FFC14A), J. Inorg. Biochem. 100 (5) (2006) 891–904, doi:10.1016/j.jinorgbio.2006.02.013; (d) F. Piccioli, S. Sabatini, L. Messori, P. Orioli, C.G. Hartinger, B.K. Keppler, A comparative study of adduct formation between the anticancer ruthenium(III) compound HInd Trans-[RuCl4(Ind)2] and serum proteins, J. Inorg. Biochem 98 (6) (2004) 1135–1142, doi:10.1016/j.jinorgbio.2004.04.002.

[7] (a) M.R. Berger, F.T. Garzon, B.K. Keppler, D. Schmähl, Efficacy of new ruthenium complexes against chemically induced autochthonous colorectal carcinoma in rats, Anticancer Res. 9 (3) (1989) 761–765; (b) S. Kapitza, M. Pongratz, M.A. Jakupec, P. Heffeter, W. Berger, L. Lackinger, B.K. Keppler, B. Marian, Heterocyclic complexes of ruthenium(III) induce apoptosis in colorectal carcinoma cells, J. Cancer Res. Clin. Oncol. 131 (2) (2005) 101–110, doi:10.1007/s00432-004-0617-0.

[8] (a) B. Sanna, M. Debidda, G. Pintus, B. Tadolini, A.M. Posadino, F. Bennardini, G. Sava, C. Ventura, The anti-metastatic agent imidazolium trans-imidazoledimethylsulfoxide-tetrachlororuthenate induces endothelial cell apoptosis by inhibiting the mitogen-activated protein kinase/extracellular signal-regulated kinase signaling pathway, Arch. Biochem. Biophys. 403 (2) (2002) 209–218, doi:10.1016/S0003-9861(02)00218-7; (b) G. Sava, A. Bergamo, S. Zorzet, B. Gava, C. Casarsa, M. Cocchietto, A. Furlani, V. Scarcia, B. Serli, E. Iengo, E. Alessio, G. Mestroni, Influence of chemical stability on the activity of the antimetastasis ruthenium compound NAMI-A, Eur. J. Cancer 38 (3) (2002) 427–435, doi:10.1016/S0959-049(01)00389-6.

[9] (a) M. Groessl, C.G. Hartinger, P.J. Dyson, B.K. Keppler, CZE–ICP-MS as a tool for studying the hydrolysis of ruthenium anticancer drug candidates and their reactivity towards the DNA Model Compound DGMP, J. Inorg. Biochem. 102 (5) (2008) 1060–1065, doi:10.1016/j.jinorgbio.2007.11.018; (b) M. Groessl, Y.O. Tsybin, C.G. Hartinger, B.K. Keppler, P.J. Dyson, Ruthenium versus platinum: interactions of anticancer metallodrugs with duplex oligonucleotides characterised by electrospray ionisation mass spectrometry, JBIC J. Biol. Inorg. Chem. 15 (5) (2010) 677–688, doi:10.1007/s00775-010-0635-0.

[10] (a) M.A. Jakupec, E. Reisner, A. Eichinger, M. Pongratz, V.B. Arion, M. Galanski, C.G. Hartinger, B.K. Keppler, Redox-active antineoplastic ruthenium complexes with indazole: correlation of *in vitro* potency and reduction potential, J. Med. Chem. 48 (8) (2005) 2831–2837, doi:10.1021/jm0490742; (b) K.K. Millis, K.H. Weaver, D.L. Rabenstein, Oxidation/reduction potential of glutathione, J. Org. Chem. 58 (15) (1993) 4144–4146, doi:10.1021/jo00067a060; (c) E. Reisner, V.B. Arion, A. Eichinger, N. Kandler, G. Giester, A.J.L. Pombeiro, B.K. Keppler, Tuning of redox properties for the design of ruthenium anticancer drugs: part 2. Syntheses, crystal structures, and electrochemistry of potentially antitumor [RuIII/IICl6-n(Azole)n]z (n = 3, 4, 6) complexes, Inorg. Chem. 44 (19) (2005) 6704–6716, doi:10.1021/ic0503737; (d) E. Reisner, V.B. Arion, M.F.C. Guedes da Silva, R. Lichtenecker, A. Eichinger, B.K. Keppler, V.Y. Kukushkin, A.J.L Pombeiro, Tuning of redox potentials for the design of ruthenium anticancer drugs – an electrochemical study of [Trans-RuCl4L(DMSO)]- and [Trans-RuCl4L2]- complexes, where L = Imidazole, 1,2,4-triazole, indazole, Inorg. Chem. 43 (22) (2004) 7083–7093, doi:10.1021/ic049479c; (e) R.L.S.R. Santos, R. van Eldik, Silva de Oliveira, D. Kinetic, Mechanistic studies on reactions of Diruthenium(Ii,Iii) with biologically relevant reducing agents, Dalton Trans. 42 (48) (2013) 16796–16805, doi:10.1039/C3DT51763B; (f) P. Schluga, C.G. Hartinger, A. Egger, E. Reisner, M. Galanski, M.A. Jakupec, B.K. Keppler, Redox behavior of tumor-inhibiting ruthenium(Iii) complexes and effects of physiological reductants on their binding to GMP, Dalton Trans. 14 (2006) 1796–1802, doi:10.1039/B511792E.

[11] (a) M.J. Clarke, V.M. Bailey, P.E. Doan, C.D. Hiller, K.J. LaChance-Galang, H. Daghlian, S. Mandal, C.M. Bastos, D. Lang, 1H NMR, EPR, UV−Vis, and Electrochemical Studies of Imidazole Complexes of Ru(III). Crystal Structures of Cis-[(Im)2(NH3)4RuIII]Br3 and [(1MeIm)6RuII]Cl2·2H2O, Inorg. Chem. 35 (17) (1996) 4896–4903, doi:10.1021/ic960355c; (b) M. Hartmann, K.-G. Lipponer, B.K Keppler, M. Alagesan, P. Sathyadevi, P. Krishnamoorthy, N.S.P. Bhuvanesh, N. Dharmaraj, Imidazole Release from the Antitumor-Active Ruthenium Complex Imidazolium Trans-Tetrachlorobis(Imidazole) Ruthenate(III) by Biologically Occurring Nucleophiles, InorganicaChim. Acta 267 (1) (1998) 137–141. DMSO Containing Ruthenium(Ii) Hydrazone Complexes: In Vitro Evaluation of Biomolecular Interaction and Anticancer Activity. Dalt. Trans. 2014, 43 (42), 15829–15840, doi:10.1016/S0020-1693(97)05556-4.

[12] (a) M. Alagesan, N.S.P. Bhuvanesh, N. Dharmaraj, Potentially cytotoxic new copper(II) hydrazone complexes: synthesis, crystal structure and biological properties, Dalton Trans. 42 (19) (2013) 7210–7223, doi:10.1039/C3DT50371B; (b) E. Jayanthi, S. Kalaiselvi, V.V. Padma, N.S.P. Bhuvanesh, N. Dharmaraj, Solvent assisted formation of ruthenium(III) and ruthenium(II) hydrazone complexes in one-pot with potential *in vitro* cytotoxicity and enhanced LDH, NO and ROS release, Dalton Trans. 45 (4) (2016) 1693–1707, doi:10.1039/C5DT03849A; (c) P. Sathyadevi, P. Krishnamoorthy, N.S.P. Bhuvanesh, P. Kalaiselvi, V. Vijaya Padma, N. Dharmaraj, Organometallic ruthenium(II) complexes: synthesis, structure and influence of substitution at azomethine carbon towards DNA/BSA binding, radical scavenging and cytotoxicity, Eur. J. Med. Chem. 55 (2012) 420–431, doi:10.1016/j.ejmech.2012.08.001.

[13] E. Jayanthi, M. Venkataramana, S. Neethu, N.S.P. Bhuvanesh, N. Dharmaraj, Biomolecular interaction and *in vitro* cytotoxicity of ruthenium complexes containing heterocyclic hydrazone. Is methanol a non-innocent solvent to influence the oxidation state of the metal and ligation of hydrazone? Polyhedron 132 (2017) 39–52, doi:10.1016/j.poly.2017.04.026.

[14] J. Chatt, G.J. Leigh, D.M.P. Mingos, R.J. Paske, Complexes of osmium, ruthenium, rhenium, and iridium halides with some tertiary monophosphines and monoarsines, J. Chem. Soc. A Inorg. Phys. Theor. (0) (1968) 2636–2641, doi:10.1039/J19680002636.

[15] E. Alessio, Synthesis and reactivity of Ru-, Os-, Rh-, and Ir-Halide−Sulfoxide complexes, Chem. Rev. 104 (9) (2004) 4203–4242, doi:10.1021/cr0307291.

[16] N.A. Mangalam, S. Sivakumar, S.R. Sheeja, M.R. PrathapachandraKurup, E.R.T. Tiekink, Chemistry of molecular and supramolecular structures of vanadium(IV) and dioxygen-bridged V(V) complexes incorporating tridentate hydrazone ligands, Inorg. Chim. Acta 362 (11) (2009) 4191–4197, doi:10.1016/j.ica.2009.06.029.

[17] APEX2, Program for data collection and integration on area detectors, in: BRUKER AXS Inc., 5465 East Cheryl Parkway, Madison, WIUSA, 1998, pp. 53711–55373.

[18] G.M. SheldrickSADABS, Program for absorption correction of area detector frames, in: BRUKER AXS Inc., 5465 East Cheryl Parkway, Madison, WIUSA, 2008, pp. 53711–55373.

[19] G.M. Sheldrick, Crystal structure refinement with {\it SHELXL}, Acta Crystallogr. Sect. C 71 (1) (2015) 3–8, doi:10.1107/S2053229614024218.

[20] L.J. Barbour, X-seed – a software tool for supramolecular crystallography, J. Supramol. Chem. 1 (4) (2001) 189–191, doi:10.1016/S1472-7862(02)00030-8.

[21] Jr M.J. Frisch, G.W. Trucks, H.B. Schlegel, G.E. Scuseria, M.A. Robb, J.R. Cheeseman, J.A. Montgomery, T. Vreven, K.N. Kudin, J.C. Burant, J.M. Millam, S.S. Iyengar, J. Tomasi, V. Barone, B. Mennucci, M. Cossi, G. Scalmani, N. Rega, G.A. Petersson, H. Nakatsuji, M. Hada, M. Ehara, K. Toyota, R. Fukuda, J. Hasegawa, M. Ishida, T. Nakajima, Y. Honda, O. Kitao, H. Nakai, M. Klene, X. Li, J.E. Knox, H.P. Hratchian, J.B. Cross, V. Bakken, C. Adamo, J. Jaramillo, R. Gomperts, R.E. Stratmann, O. Yazyev, A.J. Austin, R. Cammi, C. Pomelli, J.W. Ochterski, P.Y. Ayala, K. Morokuma, G.A. Voth, P. Salvador, J.J. Dannenberg, V.G. Zakrzewski, S. Dapprich, A.D. Daniels, M.C. Strain, O. Farkas, D.K. Malick, A.D. Rabuck, K. Raghavachari, J.B. Foresman, J.V. Ortiz, Q. Cui, A.G. Baboul, S. Clifford, J. Cioslowski, S.B.B. Tefanov, G. Liu, A. Liashenko, P. Piskorz, I. Komaromi, R.L. Martin, D.J. Fox, T. Keith, M.A. AlLaham, C.Y. Peng, A. Nanayakkara, M. Challacombe, P.M.W. Gill, B. Johnson, W. Chen, M.W. Wong, C. Gonzalez, J.A. Pople, Gaussian 03, Revision C.02 Gaussian, Inc, Wallingford, CT, 2004.

[22] (a) A. KhelifaBaghdouche, S. Mosbah, Y. Belhocine, L. Bencharif, Zwitterionic 1-{(E)-[(2-methyl-phen-yl)iminium-yl]meth-yl}naphthalen-2-olate, Acta Crystallogr. Sect. E 70 (6) (2014) o676, doi:10.1107/S1600536814008794; (b) B. Annaraj, M.A. Neelakantan, Water-soluble pyridine-based colorimetric chemosensor for naked eye detection of silver ions: design, synthesis, spectral and theoretical investigation, Anal. Methods 6 (24) (2014) 9610–9615, doi:10.1039/C4AY01592D.

[23] M.E. Reichmann, S.A. Rice, C.A. Thomas, P. Doty, A further examination of the molecular weight and size of desoxypentose nucleic acid, J. Am. Chem. Soc. 76 (11) (1954) 3047–3053, doi:10.1021/ja01640a067.
[24] O.V. Dolomanov, L.J. Bourhis, R.J. Gildea, J.A.K. Howard, H. Puschmann, {\it OLEX2}: a complete structure solution, refinement and analysis program, J. Appl. Crystallogr. 42 (2) (2009) 339–341, doi:10.1107/S0021889808042726.
[25] J.B. Chaires, N. Dattagupta, D.M. Crothers, Studies on interaction of anthracycline antibiotics and deoxyribonucleic acid: equilibrium binding studies on the interaction of daunomycin with deoxyribonucleic acid, Biochemistry 21 (17) (1982) 3933–3940, doi:10.1021/bi00260a005.
[26] (a) A. Wolfe, G.H. Shimer, T. Meehan, Polycyclic aromatic hydrocarbons physically intercalate into duplex regions of denatured DNA, Biochemistry 26 (20) (1987) 6392–6396, doi:10.1021/bi00394a013; (b) P. Krishnamoorthy, P. Sathyadevi, A.H. Cowley, R.R. Butorac, N. Dharmaraj, Evaluation of DNA binding, DNA cleavage, protein binding and *in vitro* cytotoxic activities of bivalent transition metal hydrazone complexes, Eur. J. Med. Chem. 46 (8) (2011) 3376–3387, doi:10.1016/j.ejmech.2011.05.001.
[27] P. Sathyadevi, P. Krishnamoorthy, R.R. Butorac, A.H. Cowley, N. Dharmaraj, Synthesis of novel heterobimetallic copper(I) hydrazone Schiff base complexes: a comparative study on the effect of heterocyclic hydrazides towards interaction with DNA/protein, free radical scavenging and cytotoxicity†, Metallomics 4 (5) (2012) 498–511, doi:10.1039/c2mt00004k.
[28] O. Trott, A.J. Olson, AutoDock vina: improving the speed and accuracy of docking with a new scoring function, efficient optimization, and multithreading, J. Comput. Chem. 31 (2) (2010) 455–461, doi:10.1002/jcc.21334.
[29] O. Trott, A.J. Olson, AutoDock Vina: improving the speed and accuracy of docking with a new scoring function, efficient optimization, and multithreading, J. Comput. Chem. 31 (2) (2010) 455–461, doi:10.1002/jcc.21334.
[30] T. Mosmann, Rapid colorimetric assay for cellular growth and survival: application to proliferation and cytotoxicity assays, J. Immunol. Methods 65 (1) (1983) 55–63, doi:10.1016/0022-1759(83)90303-4.
[31] M. Venkataramana, S. Chandra Nayaka, T. Anand, R. Rajesh, M. Aiyaz, S.T. Divakara, H.S. Murali, H.S. Prakash, P.V. Lakshmana Rao, Zearalenone induced toxicity in SHSY-5Y cells: the role of oxidative stress evidenced by N-acetyl cysteine, Food Chem. Toxicol. 65 (2014) 335–342, doi:10.1016/j.fct.2013.12.042.
[32] Z.H. Chohan, M.A. Farooq, A. Scozzafava, C.T. Supuran, Antibacterial Schiff bases of oxalyl-hydrazine/diamide incorporating pyrrolyl and salicylyl moieties and of their zinc(II) complexes, J. Enzyme Inhib. Med. Chem. 17 (1) (2002) 1–7, doi:10.1080/14756360290005598.
[33] N. Chitrapriya, V. Mahalingam, M. Zeller, R. Jayabalan, K. Swaminathan, K. Natarajan, Synthesis, crystal structure and biological activities of dehydroacetic acid complexes of Ru(II) and Ru(III) containing PPh3/AsPh3, Polyhedron 27 (3) (2008) 939–946, doi:10.1016/j.poly.2007.11.039; (b) R.S. Srivastava, F.R. Fronczek, Synthesis and crystal structures of carbonyl derivatives of chloride–tetramethylene sulfoxide–ruthenium(III) complexes: $[RuCl_3(TMSO)_2(CO)]$ and $[H(TMSO)_2]$ $[RuCl_4(TMSO)(CO)]$, Inorg. Chim. Acta 322 (1) (2001) 32–36, doi:10.1016/S0020-1693(01)00529-1; (c) A. Hijazi, J.P. Djukic, M. Pfeffer, L. Ricard, N. Kyritsakas-Gruber, J. Raya, P. Bertani, A. de Cian, Direct orthoruthenation of planar prochiral pyridine derivatives by C−H bond activation with $[Ru(CO)_2Cl_2]$n and its unexpected stereoselectivity, Inorg. Chem. 45 (12) (2006) 4589–4591, doi:10.1021/ic0604112.
[34] N. Chitrapriya, V. Mahalingam, M. Zeller, K. Natarajan, Synthesis, characterization and crystal structures of cyclometallatedRu(II) carbonyl complexes formed by hydrazones, Polyhedron 27 (6) (2008) 1573–1580, doi:10.1016/j.poly.2008.01.032.
[35] T.S. Kamatchi, N. Chitrapriya, H. Lee, C.F. Fronczek, F.R. Fronczek, K. Natarajan, Ruthenium(II)/(III) complexes of 4-hydroxy-pyridine-2,6-dicarboxylic acid with PPh3/AsPh3 as Co-ligand: impact of oxidation state and co-ligands on anticancer activity *in vitro*, Dalton Trans. 41 (7) (2012) 2066–2077, doi:10.1039/C1DT11273B.
[36] J. Matijević-Sosa, M. Vinković, D. Vikić-Topić, NMR Spectroscopy of 2-hydroxy-1-naphthylidene Schiff bases with chloro and hydroxy substituted aniline moiety, Croat. Chem. Acta 79 (3) (2006) 489–495; (b) M. Vieites, P. Buccino, L. Otero, M. González, O.E. Piro, R. Sánchez Delgado, C.M.R. Sant' Anna, E.J. Barreiro, H. Cerecetto, D. Gambino, Chemo-selective hydrolysis of the iminic moiety in salicylaldehyde semicarbazone promoted by ruthenium, Inorg. Chim. Acta 358 (11) (2005) 3065–3074, doi:10.1016/j.ica.2005.04.021.
[37] V. Mahalingam, N. Chitrapriya, F.R. Fronczek, K. Natarajan, New Ru(II)–DMSO complexes of ON/SN chelates: synthesis, behavior of schiff bases towards hydrolytic cleavage of CN bond, electrochemistry and biological activities, Polyhedron 29 (18) (2010) 3363–3371, doi:10.1016/j.poly.2010.09.019.
[38] N. Ahmed, J.J. Levison, S.D. Robinson, M.F. Uttley, Complexes of Ruthenium, Osmium, Rhodium, and Iridium Containing Hydride Carbonyl, or Nitrosyl Ligands, Inorg. Synth. 15 (1974) 48–59.
[39] M.B. Dinger, J.C. Mol, Degradation of the first-generation grubbs metathesis catalyst with primary alcohols, water, and oxygen. Formation and catalytic activity of ruthenium(II) monocarbonyl species, Organometallics 22 (5) (2003) 1089–1095, doi:10.1021/om0208218.
[40] C.S. Yi, D.W. Lee, Y. Chen, Hydrovinylation and [2+2] cycloaddition reactions of alkynes and alkenes catalyzed by a well-defined cationic ruthenium−alkylidene complex, Organometallics 18 (11) (1999) 2043–2045, doi:10.1021/om990129l.
[41] J.K. Barton, A. Danishefsky, J. Goldberg, Tris(Phenanthroline)Ruthenium(II): stereoselectivity in binding to DNA, J. Am. Chem. Soc. 106 (7) (1984) 2172–2176, doi:10.1021/ja00319a043.
[42] Q. Zhang, J. Liu, H. Chao, G. Xue, L. Ji, DNA-binding and photocleavage studies of cobalt(III) polypyridyl complexes:, J. Inorg. Biochem. 83 (2001) 49–55.
[43] (a) G.Z. Chen, X.Z. Huang, Z.Z. Zheng, J.G. Xu, Z.B. Wang, Methods of Fluorescence Analysis, 2nd Science Press, Beijing, 1990; (b) E.K. Efthimiadou, A. Karaliota, G. Psomas, Metal complexes of the third-generation quinolone antimicrobial drug sparfloxacin: structure and biological evaluation, 2010 J. Inorg. Biochem., 104 455–466, doi:10.1016/j.jinorgbio.2009.12.019.
[44] (a) E.C. Long, J.K. Barton, On demonstrating DNA intercalation, Acc. Chem. Res. 23 (9) (1990) 271–273, doi:10.1021/ar00177a001; (b) S. Arounaguiri, B.G. Maiya, Electro-photo switch" and "molecular light switch" devices based on ruthenium(II) complexes of modified dipyridophenazine ligands: modulation of the photochemical function through ligand design, Inorg. Chem. 38 (5) (1999) 842–843, doi:10.1021/ic981109z.
[45] M.K. Tanimoto, K. Dias, S. Dovidauskas, S. Nikolaou, Tuning the reaction products of ruthenium and ciprofloxacin for studies of DNA interactions, J. Coord. Chem. 65 (9) (2012) 1504–1517, doi:10.1080/00958972.2012.675434.
[46] F.J. Meyer-Almes, D. Porschke, Mechanism of intercalation into the DNA double helix by ethidium, Biochemistry 32 (16) (1993) 4246–4253, doi:10.1021/bi00067a012.
[47] Q. Zhang, F. Zhang, W. Wang, X. Wang, Synthesis, crystal structure and DNA binding studies of a binuclear copper(II) complex with phenanthroline, J. Inorg. Biochem. 100 (8) (2006) 1344–1352, doi:10.1016/j.jinorgbio.2006.03.010; (b) M. Alagesan, P. Sathyadevi, P. Krishnamoorthy, N.S.P. Bhuvanesh, N. Dharmaraj, DMSO containing ruthenium(II) hydrazone complexes: *in vitro* evaluation of biomolecular interaction and anticancer activity, Dalton Trans. 43 (42) (2014) 15829–15840, doi:10.1039/C4DT01032A; (c) D.S. Raja, N.S.P. Bhuvanesh, K. Natarajan, A novel water soluble ligand bridged cobalt(Ii) coordination polymer of 2-Oxo-1,2-dihydroquinoline-3-carbaldehyde (Isonicotinic) hydrazone: evaluation of the DNA binding, protein interaction, radical scavenging and anticancer activity, Dalton Trans. 41 (15) (2012) 4365–4377, doi:10.1039/C2DT12274J.
[48] M.N. Patel, H.N. Joshi, C. Patel, Cytotoxic, DNA binding, DNA cleavage and antibacterial studies of ruthenium–fluoroquinolone complexes, J. Chem. Sci. 126 (3) (2014) 739–749, doi:10.1007/s12039-014-0597-9.
[49] S.M.T. Shaikh, J. Seetharamappa, S. Ashoka, P.B. Kandagal, A study of the interaction between bromopyrogallol red and bovine serum albumin by spectroscopic methods, Dye. Pigment 73 (2) (2007) 211–216, doi:10.1016/j.dyepig.2005.11.008.
[50] D. Senthil Raja, N.S.P. Bhuvanesh, K. Natarajan, Effect of N(4)-phenyl substitution in 2-Oxo-1,2-dihydroquinoline-3-carbaldehyde semicarbazones on the structure, DNA/protein interaction, and antioxidative and cytotoxic activity of Cu(II) complexes, Inorg. Chem. 50 (24) (2011) 12852–12866, doi:10.1021/ic2020308.
[51] P. Pattanaik, G. Ravindra, C. Sengupta, K. Maithal, P. Balaram, H. Balaram, Unusual fluorescence of W168 in plasmodium falciparum triosephosphate isomerase, probed by single-tryptophan mutants, Eur. J. Biochem. 270 (4) (2003) 745–756, doi:10.1046/j.1432-1033.2003.03436.x.
[52] (a) D.C. Carter, J.X Ho, Structure of serum albumin, in: C.B. Anfinsen, J.T. Edsall, F.M. Richards, D.S.B.T.A. Eisenberg (Eds.), Lipoproteins, Apolipoproteins, and Lipases Academic Press, 1994, pp. 153–203. in P. C.Vol. 45, doi:10.1016/S0065-3233(08)60640-3; (b) Y.Q. Wang, H.M. Zhang, G.C. Zhang, W.H. Tao, S.H. Tang, Interaction of the flavonoid hesperidin with bovine serum albumin: a fluorescence quenching study, 2007 J. Lumin., 126 211–218, doi:10.1016/j.jlumin.2006.06.013; (c) P. Bolel, N. Mahapatra, M. Halder, Optical spectroscopic exploration of binding of cochineal red A with two homologous serum albumins, 2012 J. Agric. Food Chem., 60 3727–3734, doi:10.1021/jf205219w.
[53] Z. Goldouzian, F. Goldouzian, J. Chamani, The investigation of the interaction between human serum transferring with colchicine in the presence of Pb + 2 ions, Synchronous Fluoresc. Meas. 1 (2) (2011) 13–15.
[54] R.K. Murray, D.K. Granner, P.A. Mayes, V.W. Rodwell, Harper's Illustrated Biochemistry, Lange Medical Books/McGraw-Hill, New Delhi, 2003.